Available online at www.sciencedirect.com

ScienceDirect

Geochimica et Cosmochimica Acta 131 (2014) 227–246

Geochimica et Cosmochimica Acta

www.elsevier.com/locate/gca

Sulfur concentration of martian basalts at sulfide saturation at high pressures and temperatures – Implications for deep sulfur cycle on Mars

Shuo Ding *, Rajdeep Dasgupta, Kyusei Tsuno

Department of Earth Science, Rice University, 6100 Main Street, MS 126, Houston, TX 77005, USA

Received 31 May 2013; accepted in revised form 1 February 2014; available online 12 February 2014

Abstract

To constrain sulfur concentration at sulfide saturation (SCSS) of martian magmas at mantle conditions, we simulated basalt-sulfide melt equilibria using two synthesized meteorite compositions, i.e., Yamato980459 and NWA2990 in both anhydrous and hydrous conditions at 1–5 GPa and 1500–1700 °C. Our experimental results show that SCSS decreases with increasing pressure and increases with increasing temperature. Based on our experimental SCSS and those from previous low-pressure experiments on high-FeO* martian basalts, we developed a parameterization to predict martian basalt SCSS as a function of depth, temperature, and melt composition. Our model suggests that sulfur contents as high as 3500–4300 ppm can be transferred from the martian mantle to the martian exogenic system, and sulfur-rich gases might have caused the greenhouse conditions during the late Noachian. However, modeling of the behavior of sulfur along the liquid line of descent of a primitive martian basalt suggests that a fraction of the magmatic sulfur could precipitate as sulfides in the cumulates during cooling and fractional crystallization of basaltic magmas. Furthermore, the latter case is consistent with the S concentration of martian meteorites, which reflect variable amount of trapped liquid in cumulus mineral assemblage. Furthermore, our model predicts an average S storage capacity of 5700 ppm for the martian magma ocean, whereas the same for Earth is only ~860 ppm. Lastly, high SCSS of martian magma ocean and its inverse correlation with depth along the mantle liquidus could have triggered a sulfur pump where the post-core-formation magma ocean of Mars would gain sulfur through interaction with SO_2/H_2S rich nascent atmosphere.

1. INTRODUCTION

The element sulfur is thought to have a significant effect on the properties and processes of terrestrial planets from core to exosphere. For example, sulfur is thought to be an important alloying light element in metallic cores of Earth, Mars, and Mercury and thus may have a direct influence on the physical states, density, dynamical and thermal evolution of cores (Li et al., 2001; Stewart et al., 2007; Corgne et al., 2008; Dasgupta et al., 2009). Similarly, the abundance of sulfur in magmas and alloy melts influences enrichment and partitioning of other key elements in mantle, crust, and core, and between solid inner and liquid outer core (Jana and Walker, 1997; Chabot and Jones, 2003; Metrich and Mandeville, 2010; Brandon et al., 2012; Lee et al., 2012; Buono et al., 2013). Volcanically emitted sulfur also has the potential to affect climate, and thus planetary habitability, over long-time scales (Halevy et al., 2007; Johnson et al., 2008).

Sulfur cycle for Mars is of particular interest because sulfur is thought to be ubiquitous in various martian reservoirs such as the atmosphere, crust, mantle, and core as

* Corresponding author. Tel.: +1 8326232477.
E-mail address: shuo.ding@rice.edu (S. Ding).

http://dx.doi.org/10.1016/j.gca.2014.02.003
0016-7037/

revealed by data from remote sensing, from Odyssey spacecraft, Viking missions, pathfinder mission and Mars Exploration Rover mission (Clark et al., 1976; Clark and Baird, 1979; King and McLennan, 2010; Gaillard et al., 2013) and from geochemical data from meteorites (Meyer, 2012). For example, sulfur is thought to be a key light element to maintain a liquid outer core of Mars and in giving rise to an early dynamo (e.g., Schubert and Spohn, 1990; Williams and Nimmo, 2004; Stewart et al., 2007). On the other hand, although sulfur-bearing species (SO_2, H_2S) have not been detected in the present-day atmosphere of Mars, negative $\Delta^{33}S$ ($-0.5‰ \sim -1.25‰$) mass-independent sulfur isotope fractionation anomalies found in secondary sulfide in ALH84001 meteorite (>3.5 Ga) and in sulfate of 1.4 Ga Nakhla meteorite (Farquhar et al., 2007; King and McLennan, 2010) are best explained by photochemical reactions. These sulfur isotope data suggest that atmospheric SO_2/H_2S could be part of sulfur cycle on Mars back in time and sulfur-rich gases could have affected early martian climate system (e.g., Halevy et al., 2007; Johnson et al., 2008). Indeed, sulfate deposits are present on Noachian to early Hesperian age (>3.5 Ga) martian surfaces, suggesting that ancient atmosphere-hydrosphere-crust interactions may have crucial in sedimentary sulfate deposition (Gendrin et al., 2005). Central to the question of distribution of sulfur among various martian reservoirs from core to atmosphere through time is the sulfur content of the bulk Mars and its silicate mantle.

Estimates of sulfur concentration of Mars by previous studies vary from 2.1 to 4.8 wt.% S depending on different accretion models (Dreibus and Wanke, 1985; Lodders and Fegley, 1997; Sanloup et al., 1999). The distribution of this budget of sulfur among various martian reservoirs is unclear. The estimate for near-surface sulfur concentration on Mars varies from 1.1 wt.% in surface basalts to >3 wt.% in soils, globally averaging in 1.76 wt.% (McLennan et al., 2010). Elevated sulfur concentration in martian meteorites (up to 2700 ppm, Meyer, 2012) suggests sulfur-enriched silicate interior as well (King and McLennan, 2010). The metallic core is also thought to be sulfur-rich. According to the solar tidal deformation (Yoder et al., 2003), moment of inertia (Longhi et al., 1992), and the strongly magnetized ancient crust of Mars obtained from the analysis of Mars Global Surveyor mission (Stevenson, 2001; Williams and Nimmo, 2004), Mars appears to have a conductive, liquid outer core and a solid inner core. In this case, 10.6–16.2 wt.% sulfur in the outer core may be needed to make the liquidus in the Fe–Ni–S system lower than the estimated core temperature (Wanke and Dreibus, 1988; Lodders and Fegley, 1997; Sanloup et al., 1999; Stewart et al., 2007). Given the possibility that the martian interior contains significant quantity of sulfur, sulfur exchange between planetary interior reservoirs (mantle and core) and surface reservoirs (crust and atmosphere) through volcanic activities and surface processes might have shaped the geochemical evolution of the red planet. In particular, sulfur exchange between the interior and the exosphere might have been key in early Mars, when volcanic activity was likely much more vigorous (Kiefer et al., 2010; Gaillard et al., 2013; Grott et al., 2013). In order to constrain (1) sulfur flux from the mantle to crust and atmosphere by magmatism and degassing and (2) of the origin of primordial sulfur in early bulk silicate Mars, it is critical to know sulfur solubility in the martian magmas.

The solubility of sulfur in silicate melts has been experimentally explored in many previous studies. Experiments have been conducted on basalts, andesites, dacites and rhyolites in anhydrous and hydrous conditions, at different temperature (T), pressure (P) and oxygen fugacity (fO_2) (e.g., Luhr, 1990; Mavrogenes and O'Neill, 1999; Holzheid and Grove, 2002; Righter et al., 2009; Jégo and Dasgupta, 2013). Based on the experimental sulfur solubility data, many empirical models predicting maximum limit of sulfur content in silicate melts have been developed (Mavrogenes and O'Neill, 1999; Holzheid and Grove, 2002; O'Neill and Mavrogenes, 2002; Li and Ripley, 2005, 2009; Liu et al., 2007; Righter et al., 2009; Baker and Moretti, 2011). Because sulfur can exist in multiple valence states, sulfur speciation in silicate melts is affected by fO_2: sulfides (S^{2-}) dominate in reducing silicate melts while in more oxidized melts sulfur dissolves mainly as sulfates (S^{6+}) with transition from S^{2-} to S^{6+} taking place between FMQ + 0.5 and FMQ + 1.5 in basaltic melt (Jugo et al., 2010). Oxygen fugacity of SNC meteorites vary from FMQ + 0.46 to ~FMQ − 5 (Wadhwa, 2001; Herd et al., 2002; Sautter et al., 2002; Goodrich, 2003; McCanta et al., 2004; Herd, 2006; Karner et al., 2006; Shearer et al., 2006; Righter et al., 2008) and the melting conditions in the martian mantle is thought to be at the lower to intermediate values of this range. Thus sulfur in martian magma should be chiefly in the form of sulfide species. In this study, we therefore, focus on sulfur concentration at sulfide saturation (SCSS) in martian magmas.

Haughton et al. (1974) proposed that there is a strong positive correlation of SCSS and FeO content in the melts. This correlation has been confirmed by the later studies on SCSS (Wendlandt, 1982; Liu et al., 2007; Righter et al., 2009). Thus, high FeO concentration of martian mafic-ultramafic systems: 17–20 wt.% in shergottites (e.g. Ol-phyric shergottites, Mikouchi, 2001; Wadhwa, 2001; Barrat et al., 2002; Taylor et al., 2002; Goodrich, 2003; Greshake et al., 2004; Shearer et al., 2008; Usui et al., 2008; Bunch et al., 2009; Sarbadhikari et al., 2009; Peslier et al., 2010; Gross et al., 2011), 15–20 wt.% in surface basalts (e.g. Gusev crater: Gellert et al., 2006; Squyres et al., 2007; Ming et al., 2008; Meridiani Planum: Rieder et al., 2004) and 15.07–20.11 wt.% in the martian mantle (Morgan and Anders, 1980; Dreibus and Wanke, 1985; Ohtani and Kamaya, 1992; Lodders and Fegley, 1997; Sanloup et al., 1999), implies that a higher SCSS than that measured in terrestrial magmas may be expected. However, experimental estimates of SCSS on high FeO^* martian magmas are scarce. The study of Righter et al. (2009) is the only experimental study, to our knowledge, that provided high P–T SCSS data on Mars-relevant basaltic compositions and provided first parameterization for SCSS martian basalts. Although Righter et al. (2009) simulated basalt-sulfide melt equilibria with wide range of basalt-FeO^* contents (4.3–32.8 wt.%), the experiments of these authors were conducted at relatively low-pressures of 1 bar and 0.8 GPa. Furthermore,

no more than 10 experiments were available from the Righter et al. (2009) study that yielded basalt with FeO^* content $\geqslant$13–14 wt.% and therefore the statistical regression of Righter et al. (2009) to extrapolate the SCSS of martian basalts to deeper depths relied on earlier experimental SCSS data on low-FeO^* terrestrial basaltic compositions. The lack of experiments at high pressures (>1 GPa) on high FeO^* (>15 wt.%) melt compositions therefore may lead to significant uncertainty in the estimated SCSS for martian basalts at deeper depths (>2 GPa) using empirical model of SCSS in Righter et al. (2009). Therefore, constraining the behavior of sulfur at conditions and processes at much greater depth, such as the onset of partial melting in the upwelling martian mantle and deep martian magma oceans (Filiberto and Dasgupta, 2011; Righter and Chabot, 2011) will require newer experiments at wider range of P–T conditions.

Here we experimentally constrain the SCSS of two primitive martian meteorite compositions at high pressures (1–5 GPa) and temperatures (1500–1700 °C). The aim was to quantitatively describe the SCSS of high-FeO^* martian magmas as a function of major element melt composition, temperature and pressure for a range of magmatic conditions. Combining data from our study and those from Righter et al. (2009) we develop a new SCSS parameterization, which was then used to understand the behavior of sulfur in a martian magma ocean, martian mantle undergoing partial melting, and crystallization of mantle derived melts.

2. METHODS

2.1. Starting compositions

Two starting compositions, equivalent to olivine-phyric shergottites Yamato 980459 (hereafter Y98; ~17.53 wt.% FeO^* and ~19.64 wt.% MgO; Greshake et al., 2004) and NWA2990 (hereafter NWA; ~16.42 wt.% FeO^* and ~8.06 wt.% MgO; Bunch et al., 2009) were used for our experiments. These compositions were chosen because both of these meteorites have been argued to potentially be primary magma, derived from the martian mantle (Filiberto and Dasgupta, 2011). Two additional compositions, equivalent of Y98 + 1.11 wt.% H_2O and NWA + 1.73 wt.% H_2O were also investigated in an attempt to constrain the effect of dissolved water on SCSS. Starting compositions are listed in Table 1. The starting compositions were synthesized using reagent grade oxides and carbonates. To minimize adsorbed water, SiO_2, TiO_2, Al_2O_3, and MgO powder were each fired overnight at 1000 °C, Fe_2O_3 at 800 °C, MnO_2 at 400 °C, $CaCO_3$ at 200 °C and Na_2CO_3 and K_2CO_3 at 110 °C. After drying, all the oxides and carbonates were first mixed and ground in an agate mortar under ethanol and dried in room temperature overnight. Well mixed powders were reduced and decarbonated at 1000 °C for 24 h in a stream of CO–CO_2 gas mixture, which set the $fO_2 \approx$ FMQ − 2. For synthesizing hydrous silicate starting mixes, base silicates were initially prepared alumina-poor and then $Al(OH)_3$ was added after reduction and decarbonation to introduce H_2O and to bring up the alumina content to the desired level. Sulfur was added to all starting mixes as FeS. Mixing proportion of 70 wt.% silicate and 30 wt.% FeS was used for Y98 compositions (anhydrous and hydrous) while 85 wt.% silicate +15 wt.% FeS was used for NWA compositions (anhydrous and hydrous). Well-ground and mixed silicate powders with FeS were stored in a desiccator.

2.2. Experimental technique

Experiments were performed using piston cylinder (PC) (1–3 GPa) and Walker-style multi anvil (MA) devices (4–5 GPa) in the experimental petrology laboratory of Rice University at 1500–1700 °C (Table 2). Homogeneous mixtures of basalt + sulfide were loaded into graphite capsules with 1.0 mm (MA)–1.5 mm (PC) wall thickness to achieve experimental fO_2 below the FMQ buffer (Médard et al., 2008). PC experiments employed a 1/2" assembly with $BaCO_3$ pressure-transmititng medium, MgO spacers, and

Table 1
Starting compositions[a].

Composition	Yamato 980459[b]			NWA 2990[b]		
(wt.%)	Y98 + H_2O	Y98	Greshake et al. (2004)[c]	NWA + H_2O	NWA	Bunch et al. (2009)[c]
SiO_2	48.05	49.60	50.1	49.81	51.09	51.12
TiO_2	0.47	0.43	0.49	0.64	0.62	0.62
Al_2O_3	5.84	6.00	6.1	9.02	9.24	9.25
FeO^*	17.05	16.80	16.0	16.02	16.43	16.43
MnO	0.51	0.52	0.44	0.42	0.44	0.44
MgO	19.10	20.17	18.4	7.85	8.07	8.07
CaO	6.20	5.80	7.3	11.37	11.67	11.68
Na_2O	0.47	0.50	0.8	1.70	1.74	1.74
K_2O	0.02	0.02	0.02	0.15	0.16	0.16
P_2O_5	0.29	0.15	0.31	0.52	0.53	0.49
H_2O	2.00	–	–	2.50	–	–
Total	100.00	100.00	100.0	100.00	100.00	100.00

[a] All compositions are normalized to 100% in total. FeO^* represents total Fe expressed as FeO.
[b] Y98, Y98 + H_2O, NWA, and NWA + H_2O are the starting compositions used in this study, based on weighing.
[c] The compositions under Greshake et al. (2004) and Bunch et al. (2009) represent the literature data on compositions of Yamato980459 and NWA2990, respectively and are included for comparison.

Table 2
Summary of experimental conditions and product phases.

Run no.	Starting Mix	P (GPa)	T (°C)	t (h)	Phases[a]
B152	Y98 + H_2O	1.0	1600	2	gl + sulf
B137	Y98 + H_2O	1.5	1600	2	qx + sulf
B151	Y98 + H_2O	2.0	1600	2	qx + sulf
B159	Y98	1.0	1600	2	gl + sulf
B160	Y98	1.5	1600	2	gl + qx + sulf
B161	Y98	2.0	1600	2	qx + sulf
B162	Y98	2.5	1600	2	gl + opx + sulf
B163	NWA	1.0	1600	2	gl + sulf
B181	NWA	1.0	1600	12	gl + sulf
B167	NWA	1.5	1600	2	gl + sulf
B165	NWA	2.0	1600	2	gl + qx + sulf
B164	NWA	2.5	1600	2	qx + sulf
B191	NWA	3.0	1600	2	gl + qx + sulf
M38	NWA	4.0	1600	2	qx + sulf
M37	NWA	5.0	1600	2	qx + sulf
M36	NWA	5.0	1650	2	qx + sulf
B189	NWA	2.0	1500	2	gl + qx + sulf
B190	NWA	2.0	1550	2	gl + qx + sulf
B186	NWA	2.0	1650	2	qx + sulf
B188	NWA	2.0	1700	2	qx + sulf
B197	NWA + H_2O	1.0	1600	2	gl + sulf
B198	NWA + H_2O	1.5	1600	2	qx + sulf
B201	NWA + H_2O	2.0	1600	2	qx + sulf
B205	NWA + H_2O	2.5	1600	2	qx + sulf
B206	NWA + H_2O	3.0	1600	2	qx + sulf

[a] gl: silicate glass; sulf: sulfide melt; qx: silicate melt as an assemblage of quench crystals; opx: orthopyroxene.

straight-walled graphite furnace, following the calibration of Tsuno and Dasgupta (2011). MA experiments were conducted in an 1100-ton Walker-style device. For MA experiments, WC anvils with 12 mm truncations, cast MgO–Al_2O_3–SiO_2 octahedra with 18 mm edge lengths and integrated gasket fins, and straight-walled graphite heaters with molybdenum end rings were used. The pressure calibration for this assembly was established against multiple high-temperature fixed points (Fig. 1). Temperature was monitored and controlled with a type-C thermocouple next to the capsule and oriented axially with respect to the heater. P–T uncertainties are estimated to be ±0.1 GPa, ±12 °C for PC (Tsuno and Dasgupta, 2011) and ±0.3 GPa, ±10 °C for MA runs. Thermal gradient across a 2 mm long capsule in our MA assembly was determined using 2-pyroxene thermometer (Nickel et al., 1985) and was found to be ⩽10 °C. For all experiments, desired pressure was reached first and then samples were heated to the desired temperature at 100 °C/min, except for one longer duration experiment, where assemblies were pre-sintered to minimize leakage of sulfide melts; Table 2. Time series experiments at 1 GPa and 1600 °C showed that 2 h long experiment produced similar texture and SCSS (5000 ± 200 ppm) to that obtained from 12 h (4700 ± 200 ppm) long experiment, which indicated that 2 h is enough for sulfur to diffuse across the capsule given the high temperature conditions (T ⩾ 1500 °C; Freda et al., 2005; Behrens and Stelling, 2011). Experiments were terminated by cutting power to the heater. The estimated quench rate was ~125–150 °C/s for PC and as much as 150 °C/s for MA. Recovered samples were mounted in epoxy, and then cut longitudinally. One half was polished down to 0.3 micron using Al_2O_3 slurry on velvet cloth for electron microprobe and Raman spectroscopic analyses and if glassy melt pool was obtained, the other half was doubly polished for Fourier Transform

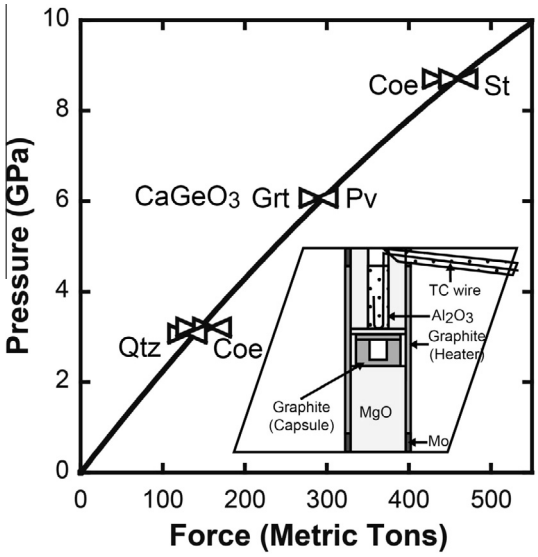

Fig. 1. Pressure calibration for the 12 mm truncated edge length (TEL) octahedral assembly (shown in inset) for the 1100-ton multi anvil press at Rice University. The force–pressure relationship was calibrated against high temperature fixed points for quartz (Qtz)–coesite (Coe) (1000 and 1200 °C) (Bose and Ganguly, 1995), $CaGeO_3$ garnet (Gt)–perovskite (Pv) (1000 °C) (Ono et al., 2011), and coesite (Coe)–stishovite (St) (1000 and 1350 °C) (Zhang et al., 1996). The fit through the brackets is described by P (GPa) = 0.023 × Force (metric tons) − 9.52 × 10^{-6} × Force (metric tons)^2.

Infrared Spectroscopy (FTIR). In order to reduce the pluck-out of sulfide blebs, vacuum impregnation with low-viscosity epoxy was performed.

2.3. Analysis of experimental samples

2.3.1. Electron microprobe

Texture and phase compositions were investigated using a Cameca SX50 electron microprobe at Texas A&M University. Samples were analyzed for major elements and S in the glassy and quenched crystal-bearing melt pool and for Fe and S in the sulfide melt. Operating conditions for silicate melt pool were accelerating voltage of 15 kV and a defocused beam of 20 μm. For each analytical point, beam current of 10 nA was first used for major elements and then 200 nA for S; for Fe and S analyses in sulfide melt, accelerating voltage of 15 kV, beam current of 20 nA and a beam of 1 or 20 μm were used. Standards used for major element analyses in silicates were natural basaltic glasses (for Mg, Si, Al, Ca), albite (Na), orthoclase (K), $SmPO_4$ (P), olivine (Fe), ilmenite (Ti) and spessartine (Mn) .For measurement of S in silicate melts, pyrite (FeS_2) was used as a primary standard and a glass of Indian Ocean basalt (USNM 113716) was used as a secondary standard. Sulfur concentration of Indian Ocean basalt that we obtained was 1140 ± 30 ppm ($n = 20$), which is similar to the previously published values of S concentration of USNM 113716 of 1160 ± 40 ppm (Jégo and Dasgupta, 2013) and also in agreement with the recommended value of ~1200 ppm. The agreement of our analyses with the recommended and published values of the standard glass lends confidence on the accuracy and reproducibility of our S analyses reported here. Both pyrite (FeS_2) and natural troilite (FeS) were used as primary standards to analyze Fe and S concentration in the sulfide melt. No measurable difference in the analyzed sulfide compositions resulted from the choice of troilite versus pyrite as analytical standard.

2.3.2. Raman spectroscopy

Raman spectroscopy, using a 514.5 nm laser, was employed to determine the speciation of sulfur dissolved in the glassy samples. Sample surface were well polished and sonicated in the ethanol bath to avoid any finger prints or other dirt. Analysis points were carefully chosen to avoid immiscible sulfide melts. Spectra were collected in the range of 100–3000 cm^{-1} with resolution of 2 cm^{-1}. Exposure times were 60 s with 10% laser power. Scans were collected five times to enhance signal-to-noise ratio. No beam damage on the sample surface was observed with these conditions, consistent with the previous studies (Klimm and Botcharnikov, 2010; Klimm et al., 2012).

2.3.3. Fourier-transformed infrared spectroscopy

A N_2 purged Thermo Nicolet Fourier Transform Infrared Spectrometer (FTIR) was used to quantify dissolved water and carbonate contents in the doubly polished experimental glasses (B152, B163, B197). Total water concentration was calculated using Beer-Lambert Law by employing molar absorption coefficient of 80 L/mol-cm (similar to 78 L/mol-cm derived by (Jendrzejewski et al., 1996) for the O–H bond stretching region from Cocheo (1994) and CO_2 content using the integrated molar absorption coefficient of carbonate doublets (284 L/mol-cm at 1500 cm^{-1} and 281 L/mol-cm at 1400 cm^{-1}) from Dixon et al. (1995). Glass density (2991, 2994, 3001 g/L for B152, B163, B197, respectively) was calculated following the protocol outlined in Silver et al. (1988). Thicknesses of doubly polished glassy samples were measured using a micronmeter and ranged from 100 to 25 μm.

3. RESULTS

3.1. Phase assemblages and texture

All experiments produced two immiscible, silicate and sulfide, quenched melts (Fig. 2a). Experiment B162 (Y98: 2.5 GPa, 1600 °C), also produced a layer of residual opx at the bottom of the capsule. Phase assemblages along with experimental conditions are given in Table 2. Sulfide saturation (Fig. 2a) was confirmed by the presence of 10–200 μm diameter, round blobs of quenched sulfide liquid embedded in the silicate melts. Three different phases were identified in large (>10 μm) quenched sulfide liquid (Fig. 2b), including light grey quenched sulfides crystals (Fe-rich, S-poor), dark grey interstitials (S-rich aggregates), and a few bright round spots (Fe-alloy with little sulfur). Sulfur in silicate melt pools was present as dissolved S in the glass (verified by Raman spectroscopy) and as discrete, sub-micron sulfide specs. The sub-micron (<0.5 μm) sulfide droplets were found to be evenly distributed and universally present in every experiment regardless of run duration and P–T condition (Fig. 2c and d). These submicron sulfides were interpreted as a phase formed during quench, and were included in the analytical volume. At low pressures (1.0 and 1.5 GPa), in addition to the sub-micron sulfide specs described above, there were a few small (1–2 μm) round sulfide droplets scattered in the silicate melts (Fig. 2c). These latter sulfide droplets were interpreted as part of the equilibrium sulfide population due to their shape, size and rarity. Therefore, microprobe spots on silicate melt pool were carefully chosen to avoid these 1–2 μm sulfide droplets. According to different compositions and run conditions, there were different textures in the quenched silicate melt (Table 2). All experiments at 1 GPa and experiments with anhydrous NWA at 1.5 and 2 GPa quenched to glass. The rest of the higher pressure experiments displayed the presence of dendritic silicates with interstitial quench sulfides (Fig. 2d). The domains with dendritic mat were avoided during analysis if glassy patches were also present in an experiment; otherwise, a defocused beam (20-40 μm) was employed to obtain average composition of the melt. Hydrous and anhydrous Y98 experiments at 1 GPa resulted in glasses within which some compositionally identical quench crystals are present. For these two compositions at higher pressures (1.5, 2.0, 2.5 GPa), dendritic quench crystals constituted the melt pool (Fig. 2d).

3.2. Spectroscopy studies

3.2.1. Raman spectra identifying sulfur speciation

Small but distinct Raman peaks around 300–400 cm^{-1} assigned to Fe–S bonds (Socrates, 2004) were observed in

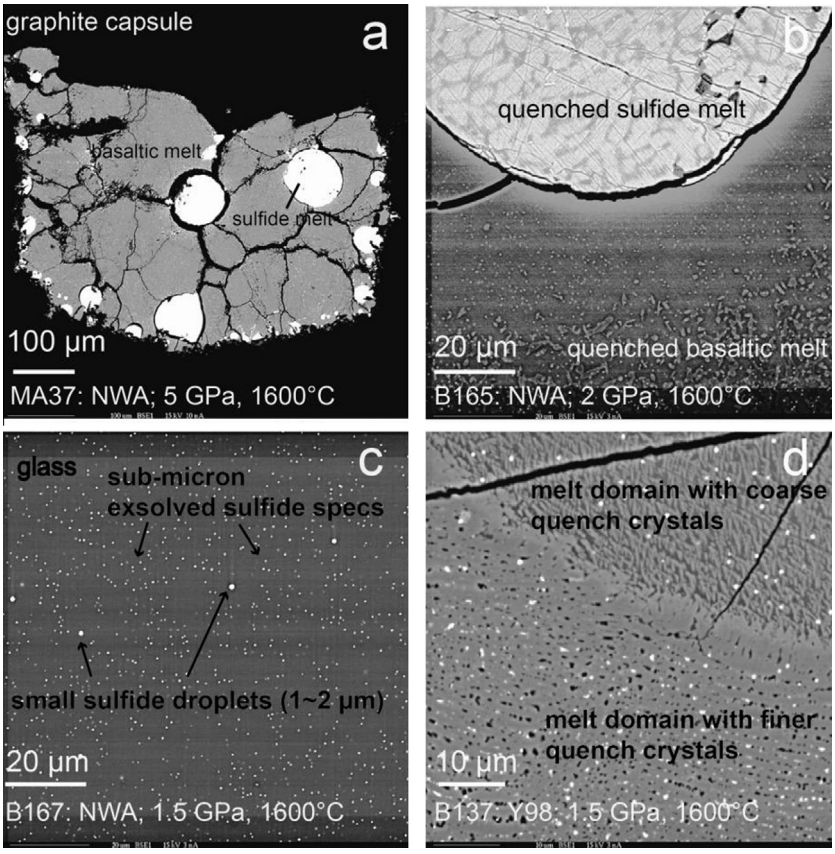

Fig. 2. Phase assemblages and texture of typical experiments, showing coexistence of equilibrium sulfide-rich and silicate-rich melts and details of quench products. (a) Round blobs of equilibrium sulfide melts embedded in basaltic silicate melt matrix. (b) Quench phases in the sulfide melt and quenched crystals and glassy patches in the silicate melt. (c) Silicate glass and submicron (<0.5 μm) sulfide specs exsolved from silicate melt during quench. Immiscible sulfide melts as small droplets (~1–2 μm) are also present. (d) Silicate melt portion of typical experiments with hydrous and anhydrous Y98 showing melt domains with both coarse and finer quench crystals.

glassy samples (B163, B167, B165; Fig. 3). These peaks matched well with that of Fe–S bond in sulfide and basalt reported by Klimm and Botcharnikov (2010). Klimm et al. (2012) has also identified S–H stretching band in Raman spectra of elemental S and H_2O– doped K_2SiO_9 glass. Overlapping bands from SH^- (at 2574 cm^{-1}, Klimm et al., 2012) and H_2S (at 2590 cm^{-1}, Klimm et al., 2012) have not been observed in our samples, indicating that S^{2-} was dominantly bound to Fe^{2+} in these high FeO basaltic melts, even though modest concentration of water was present. Peaks appearing around 800 and 1000 cm^{-1} (Fig. 3) were related to the glass structure and correspond to bridging oxygen and Si–O stretching vibrations (Klimm et al., 2012).

3.2.2. FTIR spectroscopy – quantifying H_2O and CO_2 contents

FTIR was conducted on three glassy samples of NWA, hydrous NWA and hydrous Y98 (B163, B197, B152). In all of the samples, asymmetric peak reflecting O–H stretching vibration was identified at the wave number of ~3500 cm^{-1}. In both the hydrous samples, molecular water peak was recognized at ~1600 cm^{-1}. Small but distinct stretch bands for CO_3^{2-} were located at around 1500 and 1430 cm^{-1}) for glasses in B152 and B163, which may have

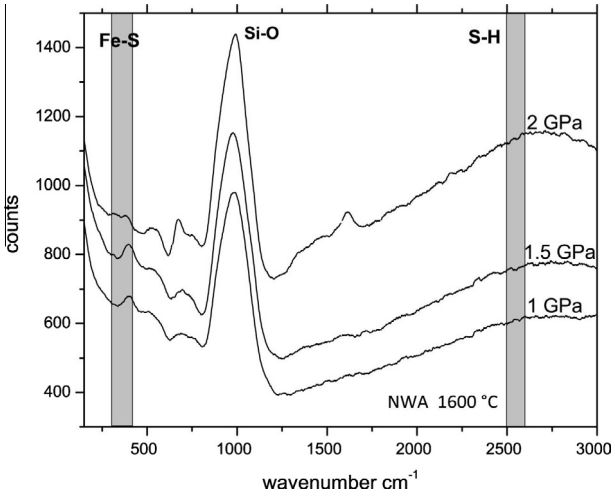

Fig. 3. Raman spectra of glassy basaltic melt with composition NWA at 1.0 (B163), 1.5 (B167), and 2.0 GPa (B165) and 1600 °C. Distinct peaks characteristic of Fe-S stretching vibration were identified in all three spectra at ~300–400 cm^{-1} and there is no obvious sign of S–H (thiol) band in the spectra. Vertical grey bands mark the position of Fe–S stretching at ~372 cm^{-1} (Klimm and Botcharnikov, 2010) and thiol at ~2574 cm^{-1} (Klimm et al., 2012).

Table 3
Phase compositions[a].

Run no.	B152	1σ	B137	1σ	B151	1σ	B159	1σ	B160	1σ	B161	1σ	B162	1σ	B163	1σ	B181	1σ
Silicate melts																		
n[b]	15		11		15		13		9		15		9		9		10	
SiO_2	48.5	0.5	47.7	0.5	47.8	0.6	50.9	0.3	49.5	0.5	49.8	0.2	48.9	0.5	46.5	0.6	47.5	0.4
TiO_2	0.36	0.04	0.37	0.07	0.35	0.05	0.4	0.1	0.38	0.07	0.52	0.06	0.47	0.04	0.65	0.05	0.63	0.06
Al_2O_3	6.1	0.1	5.8	0.1	6.3	0.2	6.02	0.08	6.2	0.1	5.8	0.2	7.1	0.1	10.0	0.2	9.9	0.1
FeO^*	14.3	0.3	15.5	0.3	14.7	0.4	15	1	13.4	0.3	17.0	0.4	17.1	0.3	16.4	0.2	12.1	0.3
MnO	0.40	0.03	0.46	0.03	0.45	0.04	0.39	0.06	0.38	0.04	0.49	0.03	0.51	0.04	0.44	0.03	0.40	0.04
MgO	20.9	0.5	21.0	0.5	21.2	0.4	18.4	0.3	20.6	0.4	19.6	0.3	17.2	0.3	9.23	0.01	11.0	0.1
CaO	6.9	0.1	6.5	0.3	6.8	0.1	6.96	0.06	7.5	0.2	6.6	0.1	7.63	0.05	12.9	0.1	15.6	0.2
Na_2O	0.54	0.06	0.50	0.05	0.61	0.05	0.47	0.04	0.45	0.03	0.53	0.07	0.60	0.05	1.78	0.09	1.78	0.04
K_2O	0.04	0.01	0.03	0.01	0.04	0.01	0.05	0.01	0.03	0.01	0.03	0.01	0.05	0.01	0.17	0.02	0.18	0.01
P_2O_5	0.15	0.03	0.16	0.04	0.18	0.04	0.16	0.04	0.17	0.04	0.17	0.04	0.19	0.06	0.55	0.04	0.48	0.04
Total	98.7	0.8	98. 6	0.8	98.7	0.7	99	1	99	1	100.9	0.4	99.9	0.5	99.1	0.8	100.0	0.5
S (ppm)	5540	940	5220	840	4380	740	4800	300	4100	300	3800	400	3500	400	5000	200	4700	200
H_2O	1.11	–	–	–	–	–	–	–	–	–	–	–	–	–	0.11	–	–	–
CO_2	0.12	–	–	–	–	–	–	–	–	–	–	–	–	–	0.07	–	–	–
Sulfide																		
n	1		6		6		8		8		17		14		3		8	
Fe	33.26	–	33.9	0.4	33.4	0.4	36	1	36	2	35	2	34.9	1.4	35	1	37.0	0.5
S	61.15	–	61.9	0.3	61.2	0.5	62.0	0.5	62.1	0.9	62.8	0.8	62.8	0.7	62.1	0.6	62.5	0.4
Total	94.41	–	95.8	0.5	94.6	0.6	98	1	98	2	98	1	98	2	97.5	0.9	99.5	0.4

Run no.	B167	1σ	B165	1σ	B164	1σ	B191	1σ	MA38	1σ	MA37	1σ	MA36	1σ	B189	1σ	B190	1σ
Silicate melts																		
n	10		11		12		19		13		13		12		15		15	
SiO_2	45.6	0.3	45.3	0.3	45.9	0.3	45.6	0.6	46.6	0.5	45.6	0.4	44.8	0.5	45.8	0.2	47.28	0.31
TiO_2	0.50	0.08	0.51	0.07	0.49	0.07	0.47	0.07	0.60	0.07	0.55	0.07	0.48	0.03	0.55	0.06	0.6	0.07
Al_2O_3	10.9	0.1	10.59	0.08	10.6	0.1	11.4	0.2	9.55	0.09	11.3	0.1	10.3	0.1	11.3	0.1	9.68	0.11
FeO^*	17.0	0.3	16.4	0.3	15.8	0.3	15.7	0.3	13.9	0.2	14.4	0.2	13.5	0.4	16.5	0.2	17.4	0.21
MnO	0.43	0.03	0.42	0.03	0.40	0.04	0.47	0.04	0.46	0.03	0.46	0.03	0.45	0.05	0.46	0.04	0.43	0.04
MgO	9.3	0.2	9.6	0.2	9.9	0.1	10.7	0.2	11.5	0.3	11.5	0.2	12.4	0.2	9.9	0.1	9.07	0.1
CaO	13.0	0.2	13. 5	0.1	13.89	0.09	14.79	0.08	13.7	0.2	14.1	0.2	14.6	0.2	13.71	0.1	13.04	0.11
Na_2O	1.65	0.05	1.69	0.04	1.64	0.08	1.63	0.06	1.43	0.06	1.44	0.07	1.4	0.1	1.67	0.05	1.71	0.06
K_2O	0.15	0.02	0.16	0.02	0.16	0.02	0.16	0.02	0.14	0.03	0.18	0.02	0.13	0.04	0.16	0.01	0.16	0.01
P_2O_5	0.56	0.06	0.56	0.04	0.59	0.07	0.63	0.04	0.52	0.05	0.61	0.05	0.58	0.07	0.62	0.06	0.52	0.04
Total	99.0	0.6	99.0	0.6	99.7	0.5	101.9	0.8	98.8	0.7	100.4	0.4	98.8	0.4	101.0	0.4	100.2	0.44
S (ppm)	4800	300	4200	300	3700	100	3000	100	3400	300	2800	100	3400	200	3300	100	3600	100
H_2O	–	–	–	–	–	–	–	–	–	–	–	–	–	–	–	–	–	
CO_2	–	–	–	–	–	–	–	–	–	–	–	–	–	–	–	–	–	
Sulfide																		
n	8		7		6		8		7		7		9		7		7	
Fe	36	1	36	1	36	2	35	2	33.1	0.6	33.9	0.3	33.6	0.8	35	1	35	2

(*continued on next page*)

Table 3 (*continued*)

Run no.	B167	1σ	B165	1σ	B164	1σ	B191	1σ	MA38	1σ	MA37	1σ	MA36	1σ	B189	1σ	B190	1σ
S	62.0	0.2	61.7	0.4	61.9	0.6	62	1	64.6	0.6	63.1	0.4	63.7	0.3	62.1	0.5	62	1
Total	98	1	97.9	0.7	98	1	97.0	0.9	97.7	0.5	97.0	0.4	97.3	0.7	97	1	97	1
Run no.	B186	1σ	B188	1σ	B197	1σ	B198	1σ	B201	1σ	B205	1σ	B206	1σ				
Silicate melts																		
n	17		15		15		24		18		16		16					
SiO_2	46.0	0.3	46.67	0.18	49.02	0.46	48.68	0.54	48	0.47	48.6	0.5	49.1	0.6				
TiO_2	0.63	0.05	0.53	0.05	0.63	0.06	0.59	0.05	0.55	0.04	0.64	0.06	0.6	0.2				
Al_2O_3	10.7	0.1	10.77	0.07	8.3	0.11	8.65	0.23	8.00	0.11	9.6	0.2	9.7	0.2				
FeO^*	17.7	0.3	17.3	0.28	15.7	0.54	16.43	0.26	14.96	0.31	16.4	0.2	16.6	0.3				
MnO	0.44	0.03	0.44	0.04	0.08	0.02	0.07	0.03	0.07	0.01	0.07	0.01	0.07	0.01				
MgO	9.5	0.2	9.58	0.15	9.92	0.2	9.88	0.39	10.73	0.13	9.0	0.2	8.7	0.5				
CaO	13.4	0.2	13.55	0.1	13.35	0.11	13.31	0.42	13.22	0.13	12.7	0.2	12.3	0.5				
Na_2O	1.7	0.07	1.62	0.08	1.87	0.09	1.21	0.17	1.42	0.17	1.36	0.09	1.4	0.2				
K_2O	0.17	0.02	0.16	0.02	0.15	0.02	0.15	0.03	0.16	0.01	0.16	0.01	0.21	0.05				
P_2O_5	0.58	0.04	0.59	0.04	0.46	0.05	0.45	0.04	0.43	0.03	0.48	0.03	0.49	0.04				
Total	101.3	0.5	101.7	0.39	99.94	0.48	99.9	0.59	97.97	0.62	99.6	0.5	99.6	0.7				
S (ppm)	4600	400	4800	500	4700	800	4900	1100	4300	400	4100	400	4100	400				
H_2O	–	–	–	–	1.73	–	–	–	–	–	–	–	–	–				
CO_2	–	–	–	–	–	–	–	–	–	–	–	–	–	–				
Sulfide																		
n	6		7		16		4		15		8		14					
Fe	35	1	33	2	34	1	35.6	0.6	35	2	35	2	35.7	0.6				
S	62.4	0.4	62.5	0.7	63.3	0.7	62.2	0.8	63	1	61.1	0.6	61.5	0.5				
Total	97.3	0.9	96	2	97.6	0.9	98	1	97.7	0.7	96	2	97.2	0.4				

[a] All concentrations are in wt.% unless otherwise noted; FeO^* represents total Fe expressed as FeO.

[b] *n* – number of electron microprobe spot analyses used to obtain the average compositions and 1σ standard deviations.

resulted from minor oxidation of graphite capsules perhaps aided by small extent of hydrogen escape. Calculations using the absorption coefficients, measured sample thicknesses, and estimated glass density, as given in the methods section, yield 0.11 wt.% H_2O in nominal anhydrous NWA (B163), and 1.73 wt.% and 1.11 wt.% H_2O in hydrous NWA (B197) and Y98 (B152), respectively. 0.07 and 0.12 wt.% CO_2 were present in anhydrous NWA (B163) and hydrous Y98 (B152), respectively.

3.3. Phase compositions

Compositions of experimental phases are given in Table 3 and SCSS data as a function of pressure and temperature, for all four starting compositions are plotted in Fig. 4.

3.3.1. Major element compositions and sulfur concentrations of silicate melts

Experimental silicate melts compositions are close to the starting composition with slight variations for each experiment. For Y98 (anhydrous and hydrous), SiO_2 and Al_2O_3 changed within 1 wt.% from ~49 to 50 wt.% and from ~6 to ~7 wt.%, respectively. FeO* varied from ~14 to ~17 wt.% while MgO from ~18 to 21 wt.%. For NWA (anhydrous and hydrous), SiO_2 ranged from ~45 to ~49 wt.% and Al_2O_3 from ~8 to ~11 wt.%. FeO* varied from ~14 to ~17 wt.% and MgO from ~9 to ~12 wt.%.

SCSS of the studied melt compositions changed systematically with change in pressure, temperature, and melt composition. At a given temperature, SCSS decreases with increasing pressure. For example, at 1600 °C, SCSS decreases from 4800 to 3500 ppm from 1.0 to 2.5 GPa for Y98, ~5440 to 4380 ppm from 1.0 to 2.0 GPa for Y98 +1.73 wt.% H_2O, 5000 to 2800 ppm from 1.0 to 5 GPa for NWA, and 4900 to 4100 ppm from 1.0 to 3.0 GPa for NWA +1.11 wt.% H_2O (Fig. 4a). At a fixed pressure, SCSS increases with increasing temperature; at 2.0 GPa and for the composition NWA, SCSS increases from 3300 to 4600 ppm from 1500 to 1700 °C (Fig. 4b). Hydrous experiments for both Y98 and NWA generated higher SCSS than those of anhydrous experiments at same *P*–*T* conditions (Fig. 4a). This implies a positive effect of water on SCSS. However, the magnitude of this positive effect varied from pressure in the experiments. The difference between SCSS of hydrous composition and that of anhydrous composition, $\Delta SCSS_{hy\text{-}anhy}$ for NWA was as high as ~1100 ppm at 3.0 GPa and only ~100 ppm at 1.5 GPa. The same type of variation was observed in case of Y98 as well. However, owing to non-glassy melt pool in many of our experiments, the water content of the resulting melt could not be directly measured and thus the effect of water on SCSS could not be quantitatively constrained.

3.3.2. Sulfide compositions

S and Fe were measured in the quenched sulfide melts. The analytical totals were 94.4–98.6 wt.% (Table 2), perhaps suggesting the presence of small amount of dissolved oxygen. A small amount of dissolved oxygen in our sulfide melt is consistent with solubility of oxygen in sulfide melts (Kress, 1997). Regardless of beam condition, atomic ratio Fe/S varied slightly from experiment to experiment, but remained mostly closely 1.

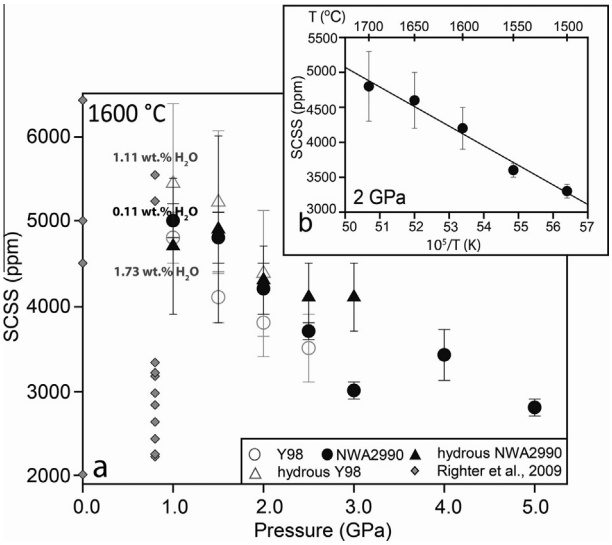

Fig. 4. Sulfur concentration at sulfide saturation (SCSS) from our experiments as a function of pressure (a) and temperature (b). (a) Experiments at 1600 °C showing a decrease in martian basalts' SCSS with increasing pressure for all four compositions (Y98, hydrous Y98, NWA2990, and hydrous NWA2990). Also shown for comparison are previous data on SCSS of model martian basalts from Righter et al. (2009) at 1 bar 0.8 GPa (grey diamonds). (b) Experiments at 2 GPa with nominally anhydrous NWA2990 showing a linear decrease in SCSS with inverse temperature.

4. DISCUSSION

4.1. SCSS – comparison to previous experimental studies

Our results showed that SCSS of martian basalts is much higher than that of terrestrial basalts investigated by previous experimental work at similar temperatures and pressures. Fig. 5a shows that at 0.8–1 GPa and 1400–1600 °C, SCSS on high-FeO* martian basalts from this study and Righter et al. (2009) are >~1000 ppm greater than experimental data from Holzheid and Grove (2002) and Liu et al. (2007). This difference is consistent with the higher FeO concentration in martian basalts. We note that the study of Righter et al. (2009), although is in broad agreement with our study, produced a larger variability of SCSS at a given FeO* content (Fig. 5a). Most of the previous models for predicting SCSS as function of *P*, *T*, and melt composition underestimate the SCSS of martian basalts as compared to our experiments (Fig. 5b). This is not surprising because the empirical parameterizations of SCSS in previous studies (Mavrogenes and O'Neill, 1999; Holzheid and Grove, 2002; O'Neill and Mavrogenes, 2002; Liu et al., 2007; Li and Ripley, 2009; Righter et al., 2009) were all built using experimental data from low-FeO* silicate melt compositions. Although the model of Righter et al. (2009) was aimed at obtaining SCSS of high-FeO* martian basalts, at high pressures (1–5.5 GPa) modeled SCSS was

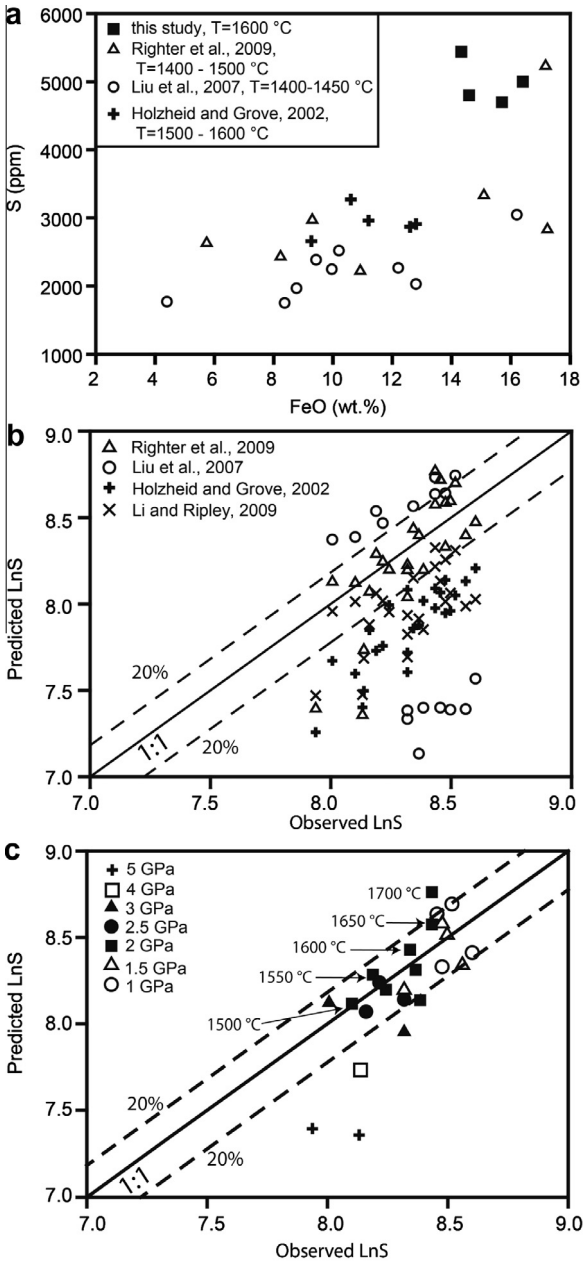

Fig. 5. (a) Comparison of experimental SCSS data on martian basalts obtained in this study with those from previous studies on terrestrial and martian basalts at similar pressures (0.8–1.0 GPa) and temperatures (1400–1600 °C). The comparison shows that high-FeO* martian basalts yield distinctly higher sulfur solubility at sulfide saturation compared to relatively low-FeO* terrestrial basalts. (b) Comparison of experimental SCSS data on martian basalts obtained in this study versus SCSS predicted for our melt compositions and experimental conditions by existing parameterization. This comparison shows that the previous parameterizations based on relatively low-FeO* basalts mostly underestimate (Holzheid and Grove, 2002; Li and Ripley, 2009) or over and underestimate (Liu et al., 2007) the SCSS of martian basalts. (c) A detailed comparison of our measurement with the model of Righter et al. (2009) shows that the latter model predicts SCSS similar to our measurements at 1–2 GPa and ⩽1600 °C, but underestimates SCSS at ⩾3 GPa (1600 °C) and overestimates SCSS ⩾ 1650 °C (2 GPa). Dashed lines indicate 20% error bounds in ppm S in melt.

calibrated on low-FeO* (<12 wt.%) melt compositions (O'Neill and Mavrogenes, 2002; Holzheid and Grove, 2002). As a result the model of Righter et al. (2009) although predicts SCSS similar to those measured in our study at 1–2 GPa, it underestimates SCSS at high pressures (>2 GPa) and overestimates SCSS at higher temperatures (>1600 °C) (Fig. 5c).

4.2. Construction of a new parameterization to predict to SCSS of martian basalts as a function of *P*, *T*, and composition

4.2.1. Thermodynamic consideration

Many previous studies discussed the possible dissolution mechanisms of sulfur in natural silicate melts and it is widely recognized that FeO* content imparts the most significant compositional control on SCSS of natural basalts (e.g., Fincham and Richardson, 1954; Haughton et al., 1974; Liu et al., 2007; Baker and Moretti, 2011). Therefore the following reaction given by Liu et al. (2007), which describes (1) a strong positive effect of FeO on SCSS and (2) the $Fe^{2+}O$ exchange between the silicate melt and a sulfide phase can be adopted to build an empirical model of SCSS

$$FeS^{sulfide} + FeO^{melt} + O^{2-,\,melt} \leftrightarrow S^{2-,\,melt} + 2FeO^{sulfide} \quad (1)$$

The equilibrium constant of the reaction in Eq. (1) at a certain P–T can be expressed as

$$K_{(1)} = \frac{a^{melt}_{S^{2-}} \cdot (a^{sulfide}_{FeO})^2}{a^{sulfide}_{FeS} \cdot a^{melt}_{FeO} \cdot a^{melt}_{O^{2-}}} \quad (2)$$

where "a" is the activity of a given component in a phase of interest (e.g., $a^{melt}_{S^{2-}}$ should be read as 'activity of S^{2-} in silicate melt'). Therefore, activity of S^{2-} in silicate melt can be written as

$$a^{melt}_{S^{2-}} = \frac{K_{(1)} \cdot a^{sulfide}_{FeS} \cdot a^{melt}_{FeO} \cdot a^{melt}_{O^{2-}}}{(a^{sulfide}_{FeO})^2} \quad (3)$$

An empirical expression of $\ln[S\text{ in ppm}]_{SCSS}$ can therefore be expressed as

$$\ln[S\text{ in ppm}]_{SCSS} = A + \frac{B}{T} + CP + D\ln(a^{melt}_{O^{2-}}) + E\ln(a^{sulfide}_{FeS}) + F\ln(a^{melt}_{FeO}) - G\ln(a^{sulfide}_{FeO}) \quad (4)$$

In this expression, the first three terms can approximately be associated with enthalpy, entropy, and the volume change of the reaction, respectively. The logarithmic terms are associated with the equilibrium constant of the sulfur dissolution reaction given in Eq. (3). Our sulfide melt analyses, in agreement with O'Neill and Mavrogenes (2002) and Mavrogenes and O'Neill (1999), suggest that $a^{sulfide}_{FeS}$ is ~1 and $a^{sulfide}_{FeO}$ is close to 0. Therefore, Eq. (4) can be simplified to

$$\ln[S\text{ in ppm}]_{SCSS} = A + \frac{B}{T} + CP + D\ln(a^{melt}_{O^{2-}}) + F\ln(a^{melt}_{FeO}) \quad (5)$$

The linear correlations between $\ln[S\text{ in ppm}]_{SCSS}$ and $1/T$ as well as $\ln[S\text{ in ppm}]_{SCSS}$ and P are consistent with our results (Fig. 4). a^{melt}_{FeO} contribution could be quantitatively

described by FeO mole fraction in the melt (X_{FeO}^{melt})and $a_{O^{2-}}^{melt}$ can either be expressed by mole fractions of other oxides (e.g., SiO_2, Al_2O_3, CaO, MgO, H_2O) which affect $\ln[S]_{SCSS}$ (Li and Ripley, 2005, 2009; Liu et al., 2007; Righter et al., 2009) or as non-bridging oxygen/total tetrahedral sites ratio (NBO/T, O'Neill and Mavrogenes, 2002).

To evaluate which combinations of oxide species or NBO/T have significant influence on martian magma SCSS, we fitted SCSS data from this study and those from Righter et al. (2009) with silicate melt FeO >10 wt.%. We used different oxides combination and NBO/T. Water contents in hydrous Y98, hydrous NWA and NWA for 1 GPa experiments were quantified by FTIR. FTIR could not be performed on Y98 because of the abundant presence of quench crystals in the silicate melt pool. However, given the small amount water (0.11 wt.%) measured in nominally anhydrous NWA, we assumed ~0.1 wt.% water for nominally dry experiments with Y98 while performing the regression. Furthermore, where no direct estimate of water content in experimental melts was available, water concentrations measured from experiments at 1 GPa for each starting material were used. This may not be accurate as some hydrogen loss or gain is possible in solid-media experiments. Therefore, further systematic experiments on hydrous glassy products would be necessary with complete quantification of both sulfur and water content in the melt.

Mole fractions of FeO (X_{FeO}^{melt}), SiO_2 ($X_{SiO_2}^{melt}$), and Al_2O_3 ($X_{Al_2O_3}^{melt}$) were found to be important variables by regression analysis while $X_{MgO}^{melt}, X_{CaO}^{melt}$, and$X_{H_2O}^{melt}$ appeared to be statistically insignificant. The fact that $X_{H_2O}^{melt}$ was found to be insignificant doesn't mean that water in melt has no effect on SCSS, obviously. This is especially so because our experimental data on average show a broad positive effect of melt water content on SCSS. We argue that because water affected SCSS by making the melts more depolymerized, water effect was incorporated in other oxide terms such as $X_{SiO_2}^{melt}$ and $X_{Al_2O_3}^{melt}$. By regression, we got the following parameterization for SCSS of martian mafic-ultramafic magmas

$$\ln[\text{S in ppm}]_{SCSS} = A + \frac{B}{T} + CP + DX_{SiO_2}^{melt} + EX_{Al_2O_3}^{melt} + F\ln(X_{FeO}^{melt}) \quad (6)$$

where the values of each of the parameters derived are given in Table 4.

Comparison of our measured SCSS with those predicted by our parameterization shows a good agreement (Fig. 6). Data set from other studies with high FeO concentration (>10 wt.%) are also plotted in Fig. 6, falling around 1:1 line within 20% error bound of sulfur concentration, indicating that our parameterization can be used to calculate SCSS of any mafic-ultramafic systems with >10 wt.% FeO. A key difference between the parameterization presented here with that of Righter et al. (2009) is that all the fitted data ($n = 35$) here are from high-FeO*, low-Al_2O_3Mars-relevant melt compositions whereas the earlier study of Righter et al. (2009) included basaltic melt with low FeO* as well. In particular, all the data at >1 GPa in Righter et al. (2009) parameterization were obtained from terrestrial basalt compositions. Hence our parameterization is an improvement over those of the previous studies specifically on martian basalt compositions.

4.3. Magmatic flux of sulfur from the martian mantle

Our experiments and parameterization of martian basalts SCSS allow us to track the behavior of sulfur in martian magmatic processes such as partial melting and fractional crystallization since sulfur behaves as a perfectly incompatible element without the presence of sulfide and its concentration in silicate melts can never exceed SCSS.

4.3.1. Extraction of magmatic S from partial melting of the martian mantle

If sulfide phases are present in the martian mantle during extraction of basaltic magma, then sulfur content of such magmas would be at the SCSS limit, which can be estimated if the magma composition and the condition of its equilibration with the mantle is known. However, depending on the extent of melting, SCSS, and bulk S content of the mantle, sulfide may be exhausted from the residual mantle; in which case S content of magma can be lower than the SCSS limit.Using a metal-silicate partition coefficient of sulfur calculated by parameterization reported in Gaillard and Scaillet (2009) and assuming a range of sulfur for the martian core, Gaillard et al. (2013) estimated that

Table 4
Coefficients of regression for SCSS parameterization.

	Coefficients	1σ[a]	Statistical fit quality parameters[b]	
A	14.25	1.57	R^2	0.7171
B	−3948.51	1851.41	F	14.7033
C	−0.06	0.05	error	0.0222
D	−2.81	2.12	p	3.31E−07
E	−7.33	3.58		
F	0.97	0.32		

For equation of the form $-\ln[\text{S in ppm}]_{SCSS} = A + \frac{B}{T} + CP + DX_{SiO_2}^{melt} + EX_{Al_2O_3}^{melt} + F\ln(X_{FeO}^{melt})$, T in Kelvin and P in GPa.

[a] 1σ Standard deviation of each coefficent reported.

[b] R^2 is the coefficient of determination, which provides a measure of how well observed outcomes are replicated by the model, as the proportion of total variation of outcomes explained by the model. The F value compares statistical models that have been fitted to a data set, in order to identify the model that best fits the population from which the data were sampled. "error" value is an estimate of the error variance for F. p indicates the probability that the null hypothesis for the full model is ture, i.e., all of the regression coefficients are zero.

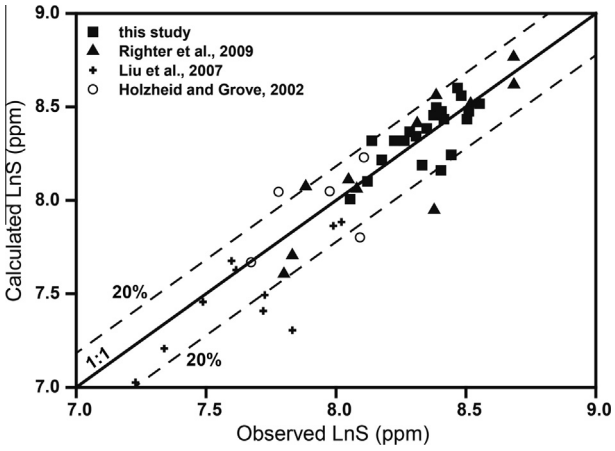

Fig. 6. Observed versus predicted $Ln[S]_{SCSS}$(ppm), testing the reliability of our parameterization against previous SCSS estimates for basalts with $FeO^* > 10$ wt.%. Experimental data for basalts with >10 wt.% FeO^* are from Righter et al. (2009), Liu et al. (2007), Holzheid and Grove (2002), and this study. Filled squares and triangles represent data from this study and Righter et al. (2009), respectively and are used to derive the parameterization. Dashed lines indicate 20% error bounds in ppm S in melt.

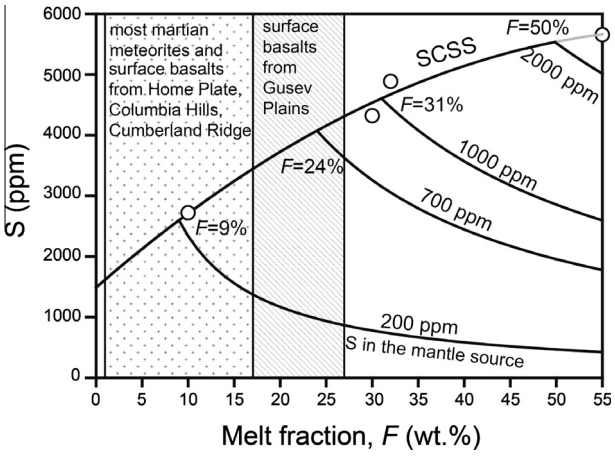

Fig. 7. S concentration in the melt (in ppm) versus melt fraction (F) during isobaric batch melting of a model martian mantle. Thick line indicates SCSS change during isobaric batch melting, which is parameterized using experimentally constrained melt composition versus F data of Bertka and Holloway (1994) at 1.5 GPa and the dependence of SCSS on P, T, and melt composition as calibrated in this study. Thin curves represent dilution of melt sulfur content after the consumption of residual sulfide for bulk martian mantle with 200, 700, 1000, and 2000 ppm S. $F = 24$ wt.% and $F = 50$ wt.% are the melt fractions at which sulfide is consumed for a mantle with 700 and 2000 ppm S, respectively. Open circles represent the available melt fraction estimates from the study of Bertka and Holloway (1994) for which SCSS were obtained using our parameterization. Also included (vertical bands) for reference are plausible melt fractions that the martian meteorites and different surface basalts may represent (e.g., Kiefer, 2003; Agee and Draper, 2004; Musselwhite et al., 2006; Filiberto and Dasgupta, 2011).

the martian mantle contains 700–2000 ppm S. This estimate has a significant uncertainty. The upper bound derives from the assumption that the bulk core contains 14.2 wt.% S (following cosmochemical considerations of Dreibus and Wanke, 1985). Similar estimate for the S abundance of the martian core has been suggested based on other geophysical constraints as well (16 ± 2 wt.% S, Rivoldini et al., 2011), justifying the choice of this upper limit of mantle S content. On the other hand, the lower bound of the martian mantle sulfur content, i.e., 700 ppm, comes from the assumption that the bulk Earth and bulk Mars contain similar S budget and the martian core contains as low as 1 wt.% S. Because of this large uncertainty in the martian mantle budget of sulfur, for the purpose of this study, we use a wider range of S content from 200 to 2000 ppm. Fig. 7 shows how sulfur content of martian mantle melt is expected to vary as a function of melting degree, based on melt compositions-melt fraction data of Bertka and Holloway (1994) at 1.5 GPa and the SCSS model developed in this study. It can be observed that if the martian mantle contains between 200 and 2000 ppm S, 9–50 wt.% melting is required (assuming an isobaric melting at ~1.5 GPa) to exhaust the sulfide phase from the residue and hence to yield magma sulfur content that is below SCSS. Fig. 7 suggests that most primitive martian basalts would be sulfide saturated, carrying ~1500–4000 ppm S, if bulk mantle S is $\geqslant$700 ppm, i.e., if extent of melting estimated from martian meteorite compositions and surface basalts are applicable (e.g., Kiefer, 2003; Agee and Draper, 2004; Musselwhite et al., 2006; Filiberto and Dasgupta, 2011). However, if the martian mantle sulfur budget is as low as that estimated for the terrestrial mantle, i.e., $\leqslant$200 ppm S (Lorand, 1990; McDonough and Sun, 1995), mantle-derived basalt could be S-poor (S content as low as ~1500–2500 ppm) for melting degree suggested for martian meteorites. Considering the lack of plate tectonics on Mars, martian mantle could have had high sulfur contents (i.e., >700 ppm) at first and then been depleted in S with melt extraction over time.

Assuming that the mantle derived basalts were sulfide saturated, we can attempt to estimate sulfur contents of various surface basalts that are argued to represent mantle-derived magmas (Monders et al., 2007; Filiberto et al., 2010; Filiberto and Dasgupta, 2011). Filiberto and Dasgupta (2011) provided 22 fractionation-corrected basalt compositions based on compositions of surface basalts from different locations in Gusev crater and Bounce Rock in Meridiani Planum and estimated conditions of their last equilibration with the mantle (Fig. 8a). For these 22 primitive compositions (FeO^* ~14–22 wt.%), we estimated their SCSS at the P–T conditions of last equilibration with the mantle. Fig. 8b shows that half of the entire primary basalts population yields SCSS of 3500–4300 ppm while a quarter of the population gives SCSS of 2700–3500 ppm. We note that this range of sulfur content is similar to that calculated for experimental partial melt compositions of Bertka and Holloway (1994), i.e., ~2700 and 4300 ppm at 10% and 30% melting, respectively. Therefore, martian magmas may carry out as much as 2700–4300 ppm sulfur at the conditions of last equilibrium with the mantle at 1–2 GPa and this entire quantity of S may potentially degas.

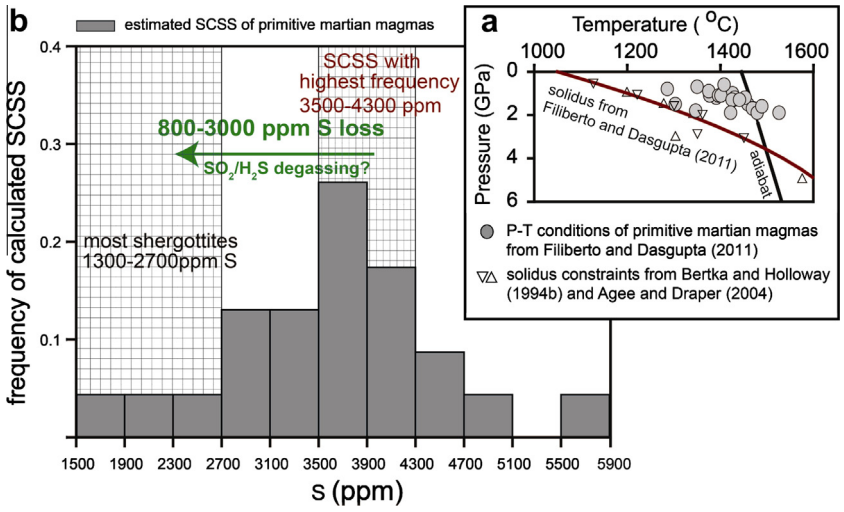

Fig. 8. (a) Estimated pressure–temperature conditions of modeled primitive martian magmas from Filiberto and Dasgupta (2011). Solid curves are martian mantle solidus fit from Filiberto and Dasgupta (2011) and martian solid mantle adiabat relevant for mantle potential temperature of 1450 °C. (b) Frequency distribution of SCSS of model martian basalts at the plausible conditions of their last equilibration with the mantle shown in (a). Shown for comparison are the available bulk S contents of shergottites (hatched area) from previous studies (e.g., Lodders 1998).

4.3.2. Fate of sulfur during fractional crystallization of martian mantle-derived primary magma

The estimate of S degassing fraction presented above is likely a maximum limit given the fact that no sulfur storage in cooled and crystallized crust is considered. A more realistic calculation should subtract the sulfur inventory of the crust, i.e., trapped in the cumulate assemblage during cooling of the magma, both as cumulus sulfide phase and dissolved in intercumulus basaltic melt. Unfortunately, no constraint on magmatic sulfur budget of the ancient martian crust exists and the only analog of Noachian crust can be various martian meteorites, though most of the latter are much younger. Comparison of our modeled SCSS and S content of martian meteorites (Dreibus et al., 1982; Laul et al., 1986; Lodders, 1998; Zipfel et al., 2000; Greshake et al., 2004; Aoudjehane et al., 2012) can place constraint on the mantle-crust exchange of sulfur on Mars and more specifically on the fraction of the mantle-liberated sulfur that may be locked in the crust owing to cooling and crystallization of the magma in more recent martian time (Hesperian and Amazonian).

Fig. 8b shows that martian meteorites contain distinctly less sulfur (800–3000 ppm S) than those that are expected from primary mantle melt at sulfide saturation. However, most meteorites are not primary magma (Filiberto and Dasgupta, 2011) and during cooling and fractional crystallization of primary magma, SCSS changes, so does the sulfur concentration in the evolving melts. In order to constrain the possible fate of sulfur dissolved in magma extracted from the mantle and emplaced into the crust, tracking sulfur concentration change during fractional crystallization of the primary melt is necessary. Though sulfur behaves incompatibly during fractional crystallization of silicates, SCSS also changes as a function of *P–T* and melt composition. Therefore, sulfide may start to precipitate if sulfur content of the differentiating magma reaches SCSS, which in turn must depend on the extent of cooling and crystallization.

To illustrate the fate of sulfur in a cooling magma, isobaric fractional crystallization calculation was performed at two distinct pressures of 0.1 and 1 GPa for starting magma composition similar to Y98 at $fO_2 = FMQ - 2$ (Fig. 9a and b) using alphaMELTS 1.2 (Smith and Asimow, 2005), a menu-driven interface of MELTS (Ghiorso and Sack, 1995; Asimow and Ghiorso, 1998) and pMELTS (Ghiorso et al., 2002). Fig. 9 shows that with a decrease in melt MgO from 20 to 4 wt.%, SCSS decreases along the liquid line of descent (LLD) from ~4262 to 2835 ppm at 1 GPa and from ~4335 to ~1524 ppm at 0.1 GPa.

If a basaltic melt started differentiating at sulfide-saturated condition, as a result of dramatic decrease of SCSS in the melt, the primitive maritan basalts would lose its sulfur by precipitating sulfides in the crystallizing assemblage. Accordingly, the bulk sulfur concentration in precipitated cumulates would increase along the cumulate line of descent. The extent of sulfur enrichment in cumulates would depend on the extent of SCSS decrease. Comparison between Fig. 9a and b reveals that more decrease of SCSS leads to more S-rich cumulates, i.e., at shallower depths. If primary melt upon emplacement in the crust is sulfide-undersaturated, sulfur concentration of the melt would first increase because of incompatible nature of sulfur till SCSS is reached (Fig. 9a and b). At what extent of fractional crystallization SCSS will be reached depends on the initial sulfur content of the melt (1000 versus 3000 ppm in Fig. 9). The more sulfur rich the starting melt is the earlier during crystallization, i.e., at a higher melt fraction and a more primitive melt composition (Fig. 9a and b), the melt would reach sulfide saturation; thus, the higher sulfur concentration could be reached in the corresponding cumulates.

Comparison of the available bulk sulfur concentration of martian meteorites to the modeled sulfur concentration

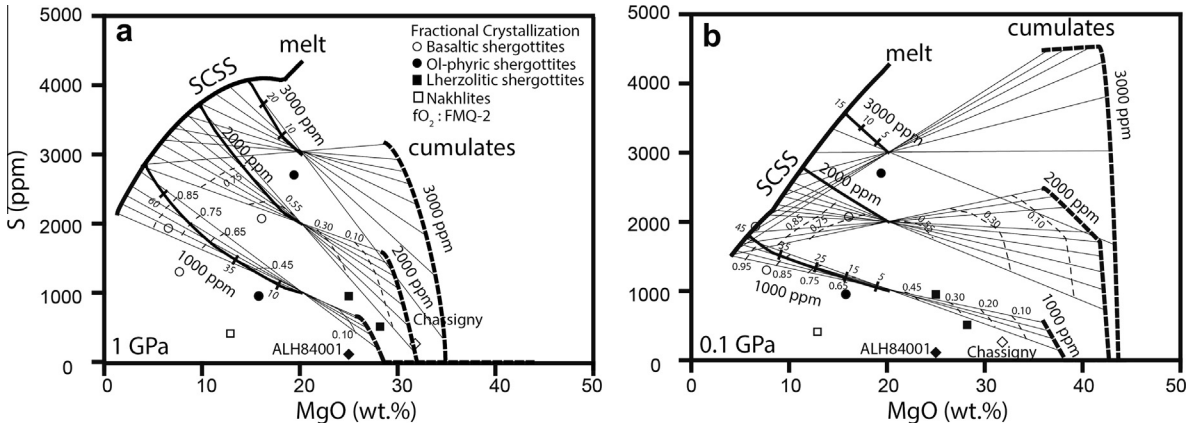

Fig. 9. Comparison of the available bulk sulfur concentration of martian meteorites to the modeled sulfur concentration in melt during fractional crystallization of Y98 at (a) 1 GPa, and (b) 0.1 GPa. Thick solid lines indicate SCSS along LLD and intermediate-thickness solid curves with numbers (1000 and 3000 ppm) represent liquids that are sulfide undersaturated to begin with. Extent of fractional crystallization is shown by tick marks along the intermediate solid curves with italic numbers. The thick dashed lines with the same number show S concentration increase in the cumulates. The thin solid lines are tie lines between liquids and corresponding cumulates. Thin dashed lines with numbers mark the melt proportions in cumulate-magma mixtures. S concentration in the martian meteorites are from Zipfel et al. (2000), Sarbadhikari et al. (2009) and Lodders (1998).

along LLD of Y98 (Fig. 9) suggests various possibilities to reconcile the sulfur "loss" showed in Fig. 9. Firstly, evolved basaltic shergottites (open circles in Fig. 9b) with high sulfur concentration can be at or close to the saturation value if crystallization happens at shallower depth (Fig. 9b). Secondly, some basaltic shergottites and olivine-phyric shergottites are on or close to the mixing lines between differentiating sulfide-saturated melt and sulfide-bearing cumulates at shallow depths (open and solid circles in Fig. 9b). Thirdly, lherzolitic shergottites (solid squares in Fig. 9a), Chassigny, and ALH 84001 with relatively low sulfur contents plotted in Fig. 9a may require mixing between sulfide-saturated melt and sulfide-bearing cumulates with low melt fractions (<0.3) at relatively deeper crystallization depths. These suggestions are consistent with previous studies, which have suggested that most shergottites are not pure liquids but contain variable amount of cumulus crystals (McCoy et al., 1999; Dann et al., 2001; Xirouchakis et al., 2002) while many other martian meteorites such as nakhlites are cumulates with variable proportion of trapped liquid (Chevrier et al., 2011). Both mesostasis sulfides as well as true intercumulus sulfide blebs have been found in shergottites and nakhlites (Lorand et al., 2005; Chevrier et al., 2011), supporting our analysis. However, most of the ultra-mafic martian meteorites (except Chassigny in Fig. 9a) appear more evolved than what is modeled in Fig. 9. This may suggest a more evolved starting melt other than Yamato980459 likely is necessary to simultaneously satisfy the major element and sulfur geochemistry of these ultramafic martian meteorites. Moreover, if mixing between sulfide-saturated differentiated melts and sulfur-bearing cumulates is responsible for sulfur contents of some martian meteorites, primary magmas of these meteorites cannot be sulfide-saturated. In the latter case, accumulated cumulates of the primary magmas would be much more sulfur rich than what is shown in Fig. 9.

The discussion above cannot rule out degassing as the cause of universally lower sulfur concentration of martian meteorites than what are modeled. However, to put lower bounds on how much sulfur could be degassed from relatively young martian basalts, more systematic calculations simulating different crystallization conditions and a more extensive database of meteorite sulfur geochemistry are necessary.

4.3.3. Degassing flux of sulfur from the martian interior

Given that sulfur contents of martian meteorites are systematically lower than the plausible range sulfur contents expected for basaltic magma at sulfide saturation, it cannot be ruled out that most of the difference in sulfur budget is degassed. $\Delta^{33}S$ anomalies in secondary sulfides in ALH84001 (>3.5 Ga, King and McLennan, 2010; Lapen et al., 2010) indicates participation of atmospheric SO_2/H_2S to surface processes in early Mars. This is consistent with the idea that magmatically-derived SO_2 may be the most important secondary green-house gas (Yung et al., 1997; Halevy et al., 2007; Johnson et al., 2008; Johnson et al., 2009), although sustained atmospheric warming by SO_2 has also been challenged owing to formation of sulfate aerosols and its shorter residence time in the atmosphere (Tian et al., 2010; McGouldrick et al., 2011).

Based on our new parameterization of SCSS of martian basalts at the conditions of their generation and their evolution during crystallization, we can place constraints on the magmatic flux of sulfur to martian exosphere. Tharsis volcanic province, formed in the late Noachian (~3.7 Ga; Carr and Head, 2010), which produced $\sim 3 \times 10^8$ km^3 of magma over 100 million years (Halevy et al., 2007), could have brought $\sim 5.7–7.0 \times 10^{13}$ g SO_2/year (assuming magma density, $\rho_{magma} = 2700$ kg/m^3) in total, if 0.35–0.43 wt.% of mantle-derived magma mass was constituted by sulfur (estimated above). However, this estimate of S degassing is a maximum limit given the fact that no sulfur

storage in the crystallized crust is considered. If the available data of sulfur content of martian meteorites of 110–2700 ppm are representative of sulfur budget of late Noachian martian crust, sulfur content of the magma that degassed could have been as low as 800–3000 ppm. Therefore, using the same parameters of magma density and magma production, the flux of sulfur during the Tharsis magmatic event becomes 1.3–3.2 $\times$ 10^{13} g SO_2/year. The maximum estimate is 1.2 times than the estimate of Halevy et al. (2007). Hence our study reinforces the idea that SO_2 and/or H_2S could have been key gases in causing the late Noachian warming and building surface sulfate deposits. We note that sulfur flux during the Noachian could have been even more dramatic, especially given the fact that degree of melting was likely more in a hotter ancient martian mantle compared to what was probably realized in the shergottite source regions (e.g., Baratoux et al., 2011; Wilson and Mustard, 2013). Owing to low solubility of carbon (e.g., Stanley et al., 2011) and high carrying capacity of sulfur in martian magma at mantle conditions (this study; Righter et al., 2009), magmatic release of sulfur-rich gases rather than carbon could have caused the warm Noachian conditions.

4.4. Sulfur in martian magma ocean

We also calculated, based on our parameterization, SCSS along liquidus and solidus of martian mantle to the estimated bottom of the martian magma ocean (Fig. 10a; 14 $\pm$ 3 GPa; Righter and Chabot, 2011; Rai and van Westrenen, 2013). Compositions of martian bulk mantle (Dreibus and Wanke, 1985) and modeled primitive melt of Yamato980459 (Filiberto and Dasgupta, 2011) were used for magma compositions along the liquidus and solidus, respectively. Similar calculation was done for the Earth (see caption of Fig. 10 for details), using the estimated base of the terrestrial magma ocean of 30 $\pm$ 3 GPa (Righter, 2011). If martian magma ocean was in equilibrium with sulfide, integrated SCSS along liquidus at 0–14 GPa gave an average S storage capacity of ~5700 ppm for martian mantle compared to that of ~860 ppm for the Earth. This is consistent with the existing cosmochemical models for the bulk Earth and Mars compositions, which suggest that Mars is richer in sulfur (Wanke and Dreibus, 1988).

High SCSS and negative correlation between SCSS and depth in martian magma ocean provide a possible way for crystallizing martian magma ocean to ingas sulfur from equilibrium SO_2/H_2S-rich primitive atmosphere after core formation (Fig. 10b; Elkins-Tanton, 2008). At low pressures, magma ocean would dissolve greater concentration of sulfur and when circulation brings a parcel of magma from to greater depths, owing to lower solubility of sulfur magma would exsolve sulfide phases. Owing to greater density, sulfide globules would segregate and eventually be trapped in the crystallizing lower mantle. After sulfide

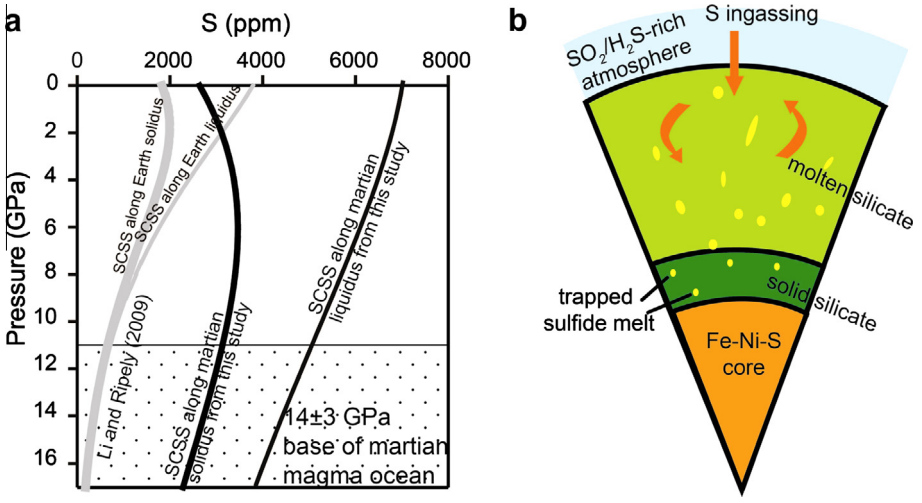

Fig. 10. (a) Estimated SCSS along liquidus and solidus of martian and terrestrial mantle. Stippled area marks the estimated depth of base of martian magma ocean based on metal-silicate partitioning of siderophile elements (14 $\pm$ 3 GPa, Righter and Chabot, 2011). (b) A cartoon cross section through martian interior, illustrating the concept of sulfur pump in a post-core formation magma ocean. Martian magma ocean has higher SCSS at shallow depths and could dissolve sulfur from atmosphere; sulfide precipitates as melt is advected to greater depths owing to diminishing SCSS. Upon ascent, silicate melt would become sulfide under-saturated and would be ready to dissolve sulfur again; precipitated sulfide droplets would be trapped in the solid silicate matrix at the base of magma ocean, enriching the bulk mantle in sulfur. Martian liquidus and solidus are taken from by Longhi et al. (1992). Composition along the martian mantle liquidus is the bulk mantle of Dreibus and Wanke (1985) and composition along the martian solidus is approximated by the composition of Yamato980459 from Filiberto and Dasgupta (2011). SCSS parameterization used for low-FeO* terrestrial mantle is from Li and Ripley (2009). Terrestrial mantle liquidus and solidus plotted here are from Takahashi (1986) and Herzberg et al. (2000), respectively. The terrestrial mantle liquidus to the base of the magma ocean was based on Herzberg et al. (2000), Zhang and Herzberg (1994), Trønnes and Frost (2002) and Fiquet et al. (2010). The silicate melt composition along the terrestrial mantle liquidus is that of fertile peridotite KLB-1 from Takahashi (1986) and the composition along the solidus of terrestrial mantle is assumed to be similar to the composition of 14 wt.% partial melt at 3 GPa from lherzolite partial melting experiments of Walter (1998).

sequestration, magma upon convective ascent would again become sulfide undersaturated and thus would be able to ingas sulfur further. This concept of magma ocean sulfur-pump is similar to magma ocean carbon-pump proposed by Dasgupta et al. (2013) as a carbon ingassing mechanism for the early Earth. Instead of being buffered by silicate-metal equilibrium, this mechanism highly depends on sulfur partitioning between molten silicate and primitive martian atmosphere. Evaluating the relative importance of sulfur partitioning between metallic alloy melt and silicate melt during core formation versus later processes such as magma ocean sulfur pump in enriching martian mantle in sulfur will require better constraint of the former. Furthermore, in order for the magma ocean sulfur pump to be effective, partial pressure of S-rich gases in the primitive atmosphere of Mars at the magma ocean stage needs to be moderately high and such constraints remain an open question at present.

5. CONCLUDING REMARKS

Our experimental determination of SCSS of FeO^*-rich basalts at high P–T (conditions relevant for melting in the martian mantle) and the following parameterization suggest that the sulfur carrying capacity of martian basalts are higher at higher pressures and lower at higher temperatures than that suggested by previous parameterization (Righter et al., 2009). The difference between our parameterization and that of Righter et al. (2009) arise from the fact that our model is built entirely on high-FeO^* martian basalts generated at 1 bar to 5 GPa whereas the Righter et al. (2009) model was calibrated on wide range of melt compositions, in particular with low-FeO^* high pressure ($\geqslant$1 Gpa) melts. Modeling SCSS using our new parameterization suggests that S-carrying capacity of martian magma ocean was at least six times greater than in the terrestrial magma ocean. This difference might have been key to make Mars a planet richer in sulfur compared to Earth. Large extent of melting of a sulfur-rich martian mantle on the other hand would be an efficient mechanism in releasing large amount of sulfur to the exosphere. Based on our new parameterization of SCSS of martian surface basalts at the estimated conditions of their generation, we placed constraints on the magmatic flux of sulfur to martian exosphere in early Mars. Our calculations strengthen some earlier suggestions that the warm Noachian greenhouse conditions could have been caused by volcanically-released S-rich gases such as SO_2 and/or H_2S. Our analysis of the fate of sulfur during cooling and crystallization of mantle-derived martian basalts at crustal conditions, however, also suggests that the impact of sulfur on the martian atmospheric chemistry could be tempered by trapping of sulfides in the crustal cumulates. In fact, sulfur geochemistry of martian meteorites suggests that most of them are not sulfide-saturated, true magmatic liquid. Instead, the available data of martian meteorites are consistent with them being crustal cumulates with silicate minerals, sulfides, and variable extent of sulfur-rich intercumulus liquid.

ACKNOWLEDGEMENTS

This manuscript benefited from constructive critique by Chusi Li, Fabrice Gaillard, and an anonymous reviewer. We also thank Marc Norman for his comments and editorial handling. The work received support from a Packard Fellowship for Science and Engineering and a NASA grant NNX13AM51G to R. D. Establishment of the Rice multi anvil facility was made possible through an NSF grant EAR-1053816 to R. D.

REFERENCES

Agee C. B. and Draper D. S. (2004) Experimental constraints on the origin of martian meteorites and the composition of the martian mantle. *Earth Planet. Sci. Lett.* **224**, 415–429.

Aoudjehane H. C., Avice G., Barrat J.-A., Boudouma O., Chen G., Duke M., Franchi I., Gattacceca J., Grady M., Greenwood R., Herd C. D. K., Hewins R., Jambon A., Marty B., Rochette P., Smith C. L., Sautter V., Verchovsky A., Weber P. and Zanda B. (2012) Tissint martian meteorite: A fresh look at the interior, surface, and atmosphere of Mars. *Science* **338**, 785–788.

Asimow P. D. and Ghiorso M. S. (1998) Algorithmic modifications extending MELTS to calculate subsolidus phase relations. *Am. Mineral.* **83**, 1127–1132.

Baker D. R. and Moretti R. (2011) Modeling the solubility of sulfur in magmas: A 50-year old geochemical challenge. *Rev. Mineral. Geochem.* **73**, 167–213.

Baratoux D., Toplis M. J., Monnereau M. and Gasnault O. (2011) Thermal history of Mars inferred from orbital geochemistry of volcanic provinces. *Nature* **472**, 338–341.

Barrat J. A., Jambon A., Bohn M., Gillet P., Sautter V., Göpel C., Lesourds M. and Keller F. (2002) Petrology and chemistry of the picritic shergottite North West Africa 1068 (NWA 1068). *Geochim. Cosmochim. Acta* **66**, 3505–3518.

Behrens H. and Stelling J. (2011) Diffusion and redox reactions of sulfur in silicate melts. *Rev. Mineral. Geochem.* **73**, 79–111.

Bertka C. M. and Holloway J. R. (1994) Anhydrous partial melting of an iron-rich mantle I: Subsolidus phase assemblages and partial melting phase relations at 10 to 30 kbar. *Contrib. Mineral Petrol.* **115**, 313–322.

Bose K. and Ganguly J. (1995) Quartz-coesite transition revisited-reversed experimental determination at 500–1200 °C and retrieved thermochemical properties. *Am. Mineral.* **80**, 231–238.

Brandon A. D., Puchtel I. S., Walker R. J., Day J. M. D., Irving A. J. and Taylor L. A. (2012) Evolution of the martian mantle inferred from the ^{187}Re–^{187}Os isotope and highly siderophile element abundance systematics of shergottite meteorites. *Geochim. Cosmochim. Acta* **76**, 206–235.

Bunch T. E., Irving A. J., Wittke J. H., Rumble D., Korotev R. L., Gellissen M. and Palme H. (2009) Petrology and composition of Northwest Africa 2990: A new type of fine-grained, enriched, olivine-phyric shergottite. *Lunar Planet. Sci. XL*. Lunar Planet. Inst., Houston. #2274 (abstr.).

Buono A. S., Dasgupta R., Lee C.-T. A. and Walker D. (2013) Siderophile element partitioning between cohenite and liquid in Fe-Ni-S-C system and implications for geochemistry of planetary cores and mantles. *Geochim. Cosmochim. Acta* **120**, 239–250.

Carr M. H. and Head J. W. (2010) Geologic history of Mars. *Earth Planet. Sci. Lett.* **294**, 185–203.

Chabot N. L. and Jones J. H. (2003) The parameterization of solid metal-liquid metal partitioning of siderophile elements. *Meteorit. Planet. Sci.* **38**, 1425–1436.

Chevrier V., Lorand J.-P. and Sautter V. (2011) Sulfide petrology of four nakhlites: Northwest Africa 817, Northwest Africa 998, Nakhla, and Governador Valadares. *Met. Planet. Sci.* **46**, 769–784.

Clark B. C. and Baird A. K. (1979) Volatiles in the Martian regolith. *Geophys. Res. Lett.* **6**, 811–814. http://dx.doi.org/10.1029/GL006i010p00811.

Clark B. C., Baird A. K., Rose, Jr, H. J., Toulmin, III, P., Keil K., Castro A. J., Kelliher W. C., Rowe C. D. and Evans P. H. (1976) Inorganic analyses of Martian surface samples at the Viking landing sites. *Science* **194**, 1283–1288.

Cocheo P. A. (1994) The solubility of water in basanitic melts at low pressures. Ph. D. thesis, Arizona State University.

Corgne A., Wood B. J. and Fei Y. (2008) C- and S-rich molten alloy immiscibility and core formation of planetesimals. *Geochim. Cosmochim. Acta* **72**, 2409–2416.

Dann J., Holzheid A., Grove T. and McSween H. (2001) Phase equilibria of the Shergotty meteorite: Constraints on pre-eruptive water contents of martian magmas and fractional crystallization under hydrous conditions. *Meteorit. Planet. Sci.* **36**, 793–806.

Dasgupta R., Buono A., Whelan G. and Walker D. (2009) High-pressure melting relations in Fe–C–S systems: Implications for formation, evolution, and structure of metallic cores in planetary bodies. *Geochim. Cosmochim. Acta* **73**, 6678–6691.

Dasgupta R., Chi H., Shimizu N., Buono A. S. and Walker D. (2013) Carbon solution and partitioning between metallic and silicate melts in a shallow magma ocean: Implications for the origin and distribution of terrestrial carbon. *Geochim. Cosmochim. Acta* **102**, 191–212.

Dixon J. E., Stolper E. M. and Holloway J. R. (1995) An experimental study of water and carbon dioxide solubilities in mid-ocean ridge basaltic liquids. Part I: Calibration and solubility models. *J. Petrol.* **36**, 1607–1631.

Dreibus G. and Wanke H. (1985) Mars, a volatile-rich planet. *Meteoritics* **20**, 367–381.

Dreibus G., Palme H., Rammensee W., Spettel B., Weckwerth G., Wanke H. (1982) Composition of Shergotty parent body: Further evidence for a two component model of planet formation. *Lunar Planet. Sci. XIII*. Lunar Planet. Inst., Houston. 186–187 (abstr.).

Elkins-Tanton L. T. (2008) Linked magma ocean solidification and atmospheric growth for Earth and Mars. *Earth Planet. Sci. Lett.* **271**, 181–191.

Farquhar J., Kim S.-T. and Masterson A. (2007) Implications from sulfur isotopes of the Nakhla meteorite for the origin of sulfate on Mars. *Earth Planet. Sci. Lett.* **264**, 1–8.

Filiberto J. and Dasgupta R. (2011) Fe^{2+}–Mg partitioning between olivine and basaltic melts: Applications to genesis of olivine-phyric shergottites and conditions of melting in the Martian interior. *Earth Planet. Sci. Lett.* **304**, 527–537.

Filiberto J., Dasgupta R., Kiefer W. S. and Treiman A. H. (2010) High pressure, near-liquidus phase equilibria of the Home Plate basalt Fastball and melting in the martian mantle. *Geophys. Res. Lett.* **37**, L13201. http://dx.doi.org/10.1029/2010GL043999.

Fincham C. and Richardson F. (1954) The behaviour of sulphur in silicate and aluminate melts. *Proc. R. Soc. London, Ser. A* **223**, 40–62.

Fiquet G., Auzende A., Siebert J., Corgne A., Bureau H., Ozawa H. and Garbarino G. (2010) Melting of peridotite to 140 gigapascals. *Science* **329**, 1516–1518.

Freda C., Baker D. R. and Scarlato P. (2005) Sulfur diffusion in basaltic melts. *Geochim. Cosmochim. Acta* **69**, 5061–5069.

Gaillard F. and Scaillet B. (2009) The sulfur content of volcanic gases on Mars. *Earth Planet. Sci. Lett.* **279**, 34–43.

Gaillard F., Michalski J., Berger G., McLennan S. M. and Scaillet B. (2013) Geochemical reservoirs and timing of sulfur cycling on Mars. *Space Sci. Rev.* **174**, 251–300.

Gellert R., Rieder R., Brückner J., Clark B. C., Dreibus G., Klingelhöfer G., Lugmair G., Ming D. W., Wänke H., Yen A., Zipfel J. and Squyres S. W. (2006) Alpha Particle X-Ray Spectrometer (APXS): Results from Gusev crater and calibration report. *J. Geophys. Res* **111**, E02S05. http://dx.doi.org/10.1029/2005JE002555.

Gendrin A., Mangold N., Bibring J.-P., Langevin Y., Gondet B., Poulet F., Bonello G., Quantin C., Mustard J., Arvidson R. and LeMouélic S. (2005) Sulfates in martian layered terrains: The OMEGA/Mars express view. *Science* **307**, 1587–1591.

Ghiorso M. S. and Sack R. O. (1995) Chemical mass transfer in magmatic processes IV. A revised and internally consistent thermodynamic model for the interpolation and extrapolation of liquid-solid equilibria in magmatic systems at elevated temperatures and pressures. *Contrib. Mineral Petrol.* **119**(5), 197–212. http://dx.doi.org/10.1029/2001GC000217.

Ghiorso M. S., Hirschmann M. M., Reiners P. W. and Kress V. C. (2002) The pMELTS: A revision of MELTS for improved calculation of phase relations and major element partitioning related to partial melting of the mantle to 3 GPa. *Geochem. Geophys. Geosyst.* **3**, 1–35.

Goodrich C. A. (2003) Petrogenesis of olivine-phyric shergottites Sayh al Uhaymir 005 and Elephant Moraine A79001 lithology A. *Geochim. Cosmochim. Acta* **67**, 3735–3772.

Greshake A., Fritz J. and Stöffler D. (2004) Petrology and shock metamorphism of the olivine-phyric shergottite Yamato 980459: Evidence for a two-stage cooling and a single-stage ejection history. *Geochim. Cosmochim. Acta* **68**, 2359–2377.

Gross J., Treiman A. H., Filiberto J. and Herd C. D. K. (2011) Primitive olivine-phyric shergottite NWA 5789: Petrography, mineral chemistry, and cooling history imply a magma similar to Yamato-980459. *Meteorit. Planet. Science* **46**, 116–133.

Grott M., Baratoux D., Hauber E., Sautter V., Mustard J., Gasnault O., Ruff S., Karato S.-I., Debaille V., Knapmeyer M., Sohl F., Van Hoolst T., Breuer D., Morschhauser A. and Toplis M. J. (2013) Long-term evolution of the martian crust-mantle system. *Space Sci. Rev.* **174**, 49–111.

Halevy I., Zuber M. T. and Schrag D. P. (2007) A sulfur dioxide climate feedback on early Mars. *Science* **318**, 1903–1907.

Haughton D. R., Roeder P. L. and Skinner B. J. (1974) Solubility of sulfur in mafic magmas. *Econ. Geol.* **69**, 451–467.

Herd C. D. (2006) Insights into the redox history of the NWA 1068/1110 martian basalt from mineral equilibria and vanadium oxybarometry. *Am. Mineral.* **91**, 1616–1627.

Herd C. D., Borg L. E., Jones J. H. and Papike J. J. (2002) Oxygen fugacity and geochemical variations in the martian basalts: Implications for martian basalt petrogenesis and the oxidation state of the upper mantle of Mars. *Geochim. Cosmochim. Acta* **66**, 2025–2036.

Herzberg C., Raterron P. and Zhang J. (2000) New experimental observations on the anhydrous solidus for peridotite KLB-1. *Geochem. Geophys. Geosyst.* **1**, Paper number 2000GC000089.

Holzheid A. and Grove (2002) Sulfur saturation limits in silicate melts and their implications for core formation scenarios for terrestrial planets. *Am. Mineral.* **87**, 227–237.

Jana D. and Walker D. (1997) The influence of silicate melt composition on distribution of siderophile elements among metal and silicate liquids. *Earth Planet. Sci. Lett.* **150**, 463–472.

Jégo S. and Dasgupta R. (2013) Fluid-present melting of sulfide-bearing ocean-crust: Experimental constraints on the transport of sulfur from slab to mantle wedge. *Geochim. Cosmochim. Acta* **110**, 106–134.

Jendrzejewski N., Javoy M. and Trull T. (1996) Mesures quantitatives de carbone et d'eau dans les verres basaltiques naturels par Spectroscopie Infrarouge. Partie II: l'eau. *Acad. Sci. II A* **322**, 735–742.

Johnson S. S., Mischna M. a., Grove T. L. and Zuber M. T. (2008) Sulfur-induced greenhouse warming on early Mars. *J. Geophys. Res.* **113**, E08005. http://dx.doi.org/10.1029/2007JE002962.

Johnson S. S., Pavlov A. a. and Mischna M. a. (2009) Fate of SO_2 in the ancient Martian atmosphere: Implications for transient greenhouse warming. *J. Geophys. Res.* **114**, E11011. http://dx.doi.org/10.1029/2008JE003313.

Jugo P. J., Wilke M. and Botcharnikov R. E. (2010) Sulfur K-edge XANES analysis of natural and synthetic basaltic glasses: Implications for S speciation and S content as function of oxygen fugacity. *Geochim. Cosmochim. Acta* **74**, 5926–5938.

Karner J. M., Sutton S. R., Papike J. J., Shearer C. K., Jones J. H. and Newville M. (2006) Application of a new vanadium valence oxybarometer to basaltic glasses from the Earth, Moon, and Mars. *Am. Mineral.* **91**, 270–277.

Kiefer W. S. (2003) Melting in the Martian mantle: Shergottite formation and implications for present-day mantle convection on Mars. *Meteorit. Planet. Sci.* **38**, 1815–1832.

Kiefer W., Li Q., Filiberto J. and Sandu C. (2010) The importance of mantle composition in controlling magma production rates on Mars and Venus. AGU Fall Meeting Abstracts, p. 05.

King P. L. and McLennan S. M. (2010) Sulfur on Mars. *Elements* **6**, 107–112.

Klimm K. and Botcharnikov R. E. (2010) The determination of sulfate and sulfide species in hydrous silicate glasses using Raman spectroscopy. *Am. Mineral.* **95**, 1574–1579.

Klimm K., Kohn S. C. and Botcharnikov R. E. (2012) The dissolution mechanism of sulphur in hydrous silicate melts. II: Solubility and speciation of sulphur in hydrous silicate melts as a function of fO_2. *Chem. Geol.* **322–323**, 250–267.

Kress V. (1997) Thermochemistry of sulfide liquids. I. The system OS-Fe at 1 bar. *Contrib. Mineral Petrol.* **127**, 176–186.

Lapen T. J., Righter M., Brandon A. D., Debaille V., Beard B. L., Shafer J. T. and Peslier A. H. (2010) A younger age of ALH84001 and its geochemical link to shergottite sources in Mars. *Science* **328**, 347–351.

Laul J., Smith M., Wänke H., Jagoutz E., Dreibus G., Palme H., Spettel B., Burghele A., Lipschutz M. and Verkouteren R. (1986) Chemical systematics of the Shergotty meteorite and the composition of its parent body (Mars). *Geochim. Cosmochim. Acta* **50**, 909–926.

Lee C.-T. A., Luffi P., Chin E. J., Bouchet R., Dasgupta R., Morton D. M., Le Roux V., Yin Q. Z. and Jin D. (2012) Copper systematics in Arc magmas and implications for crust-mantle differentiation. *Science* **336**, 64–68.

Li C. and Ripley E. M. (2005) Empirical equations to predict the sulfur content of mafic magmas at sulfide saturation and applications to magmatic sulfide deposits. *Miner. Deposita* **40**, 218–230.

Li C. and Ripley E. M. (2009) Sulfur contents at sulfide-liquid or anhydrite saturation in silicate melts: Empirical equations and example applications. *Econ. Geol.* **104**, 405–412.

Li J., Fei Y., Mao H. K., Hirose K. and Shieh S. R. (2001) Sulfur in the Earth's inner core. *Earth Planet. Sci. Lett.* **193**, 509–514.

Liu Y., Samaha N.-T. and Baker D. R. (2007) Sulfur concentration at sulfide saturation (SCSS) in magmatic silicate melts. *Geochim. Cosmochim. Acta* **71**, 1783–1799.

Lodders K. (1998) A survey of shergottite, nakhlite and chassigny meteorites whole-rock compositions. *Meteorit. Planet. Sci.* **33**, A183–A190.

Lodders K. and Fegley, Jr, B. (1997) An oxygen isotope model for the composition of Mars. *Icarus* **126**, 373–394.

Longhi J., Knittle E., Holloway J. R. and Waenke H. (1992) The bulk composition, mineralogy and internal structure of Mars. In *Mars* (eds. M. S. Matthews, H. H. Kieffer, B. M. Jakosky and C. Snyder). University of Arizona Press, Tuscon, Arizona, pp. 184–208.

Lorand J. (1990) Are spinel Iherzolite xenoliths representative of the abundance of sulfur in the upper mantle?. *Geochim. Cosmochim. Acta* **54** 1487–1492.

Lorand J.-P., Chevrier V. and Sautter V. (2005) Sulfide mineralogy and redox conditions in some shergottites. *Meteorit. Planet. Sci.* **40**, 1257–1272.

Luhr J. F. (1990) Experimental phase relations of water-and sulfur-saturated arc magmas and the 1982 eruptions of El Chichón volcano. *J. Petrol.* **31**, 1071–1114.

Mavrogenes J. A. and O'Neill H. S. C. (1999) The relative effects of pressure, temperature and oxygen fugacity on the solubility of sulfide in mafic magmas. *Geochim. Cosmochim. Acta* **63**, 1173–1180.

McCanta M. C., Dyar M. D., Rutherford M. J. and Delaney J. S. (2004) Iron partitioning between basaltic melts and clinopyroxene as a function of oxygen fugacity. *Am. Mineral.* **89**, 1685–1693.

McCoy T. J., Wadhwa M. and Keil K. (1999) New lithologies in the Zagami meteorite: Evidence for fractional crystallization of a single magma unit on Mars. *Geochim. Cosmochim. Acta* **63**, 1249–1262.

McDonough W. F. and Sun S.-S. (1995) The composition of the Earth. *Chem. Geol.* **120**, 223–253.

McGouldrick K., Toon O. B. and Grinspoon D. H. (2011) Sulfuric acid aerosols in the atmospheres of the terrestrial planets. *Planet. Space Sci.* **59**, 934–941.

McLennan S. M., Boynton W. V., Karunatillake S., Hahn B.C., Taylor G. J. and Mars Odyssey GRS Team (2010) Distribution of sulfur on the surface of Mars determined by the 2001 Mars Odyssey gammaray spectrometer. *Lunar Planet. Sci.* Lunar Planet. Inst., The Woodlands, Texas. #1533 (abstr.).

Médard E., McCammon C. A., Barr J. A. and Grove T. L. (2008) Oxygen fugacity, temperature reproducibility, and H2O contents of nominally anhydrous piston-cylinder experiments using graphite capsules. *Am. Mineral.* **93**, 1838–1844.

Metrich N. and Mandeville C. W. (2010) Sulfur in magmas. *Elements* **6**, 81–86.

Meyer, Jr., C. (2012) Website: http://curator.jsc.nasa.gov/antmet/mmc/index.cfm.

Mikouchi T. (2001) Mineralogical similarities and differences between the Los Angeles basaltic shergottite and the Asuka-881757 lunar mare meteorite. *Antarct. Meteorite Res.* **14**, 1–20.

Ming D. W., Gellert R., Morris R. V., Arvidson R. E., Brückner J., Clark B. C., Cohen B. A., d'Uston C., Economou T., Fleischer I., Klingelhöfer G., McCoy T. J., Mittlefehldt D. W., Schmidt M. E., Schröder C., Squyres S. W., Tréguier E., Yen a. S. and Zipfel J. (2008) Geochemical properties of rocks and soils in Gusev Crater, Mars: Results of the Alpha Particle X-ray spectrometer from Cumberland Ridge to Home Plate. *J. Geophys. Res.*, E12S39. http://dx.doi.org/10.1029/2008JE003195.

Monders A. G., Medard E. and Grove T. L. (2007) Phase equilibrium investigations of the Adirondack class basalts from Gusev plains, Gusev crater. *Mars. Meteorit. Planet. Sci.* **42**, 131–148.

Morgan J. W. and Anders E. (1980) Chemical composition of Earth, Venus, and Mercury. *Proc. Natl. Acad. Sci.* **77**, 6973–6977.

Musselwhite D. S., Dalton H. A., Kiefer W. S. and Treiman A. H. (2006) Experimental petrology of the basaltic shergottite Yamato-980459: Implications for the thermal structure of the Martian mantle. *Meteorit. Planet. Sci.* **41**, 1271–1290.

Nickel K. G., Brey G. P. and Kogarko L. (1985) Orthopyroxene–clinopyroxene equilibria in the system CaO–MgO–Al_2O_3–SiO_2 (CMAS): New experimental results and implications for two-pyroxene thermometry. *Contrib. Mineral. Petrol.* **91**, 44–53.

O'Neill H. and Mavrogenes J. A. (2002) The sulfide capacity and the sulfur content at sulfide saturation of silicate melts at 1400 °C and 1 bar. *J. Petrol.* **43**, 1049–1087.

Ohtani E. and Kamaya N. (1992) The geochemical model of Mars: An estimation from the high pressure experiments. *Geophys. Res. Lett.* **19**, 2239–2242. http://dx.doi.org/10.1029/92GL02369.

Ono S., Kikegawa T. and Higo Y. (2011) In situ observation of a garnet/perovskite transition in $CaGeO_3$. *Phys. Chem. Miner.* **38**, 735–740.

Peslier A., Hnatyshin D., Herd C., Walton E., Brandon A., Lapen T. and Shafer J. (2010) Crystallization, melt inclusion, and redox history of a Martian meteorite: Olivine-phyric shergottite Larkman Nunatak 06319. *Geochim. Cosmochim. Acta* **74**, 4543–4576.

Rai N. and van Westrenen W. (2013) Core-mantle differentiation in Mars. *J. Geophys. Res.* **118**, 1195–1203. http://dx.doi.org/10.1002/jgre.20093.

Rieder R., Gellert R., Anderson R. C., Brückner J., Clark B. C., Dreibus G., Economou T., Klingelhöfer G., Lugmair G. W., Ming D. W., Squyres S. W., d'Uston C., Wänke H., Yen a. and Zipfel J. (2004) Chemistry of rocks and soils at Meridiani Planum from the Alpha Particle X-ray Spectrometer. *Science* **306**, 1746–1749.

Righter K. (2011) Prediction of metal–silicate partition coefficients for siderophile elements: An update and assessment of PT conditions for metal–silicate equilibrium during accretion of the Earth. *Earth Planet. Sci. Lett.* **304**, 158–167.

Righter K. and Chabot N. L. (2011) Moderately and slightly siderophile element constraints on the depth and extent of melting in early Mars. *Meteorit. Planet. Sci.* **46**, 157–176.

Righter K., Yang H., Costin G. and Downs R. T. (2008) Oxygen fugacity in the Martian mantle controlled by carbon: New constraints from the nakhlite MIL 03346. *Meteorit. Planet. Sci.* **43**, 1709–1723.

Righter K., Pando K. and Danielson L. R. (2009) Experimental evidence for sulfur-rich martian magmas: Implications for volcanism and surficial sulfur sources. *Earth Planet. Sci. Lett.* **288**, 235–243.

Rivoldini A., Van Hoolst T., Verhoeven O., Mocquet A. and Dehant V. (2011) Geodesy constraints on the interior structure and composition of Mars. *Icarus* **213**, 451–472.

Sanloup C., Jambon A. and Gillet P. (1999) A simple chondritic model of Mars. *Phys. Earth Planet. Int.* **112**, 43–54.

Sarbadhikari A. B., Day J. M. D., Liu Y., Rumble, III, D. and Taylor L. A. (2009) Petrogenesis of olivine-phyric shergottite Larkman Nunatak 06319: Implications for enriched components in martian basalts. *Geochim. Cosmochim. Acta* **73**, 2190–2214.

Sautter V., Barrat J., Jambon A., Lorand J., Gillet P., Javoy M., Joron J. and Lesourd M. (2002) A new martian meteorite from Morocco: The nakhlite North West Africa 817. *Earth Planet. Sci. Lett.* **195**, 223–238.

Schubert G. and Spohn T. (1990) Thermal history of Mars and the sulfur content of its core. *J. Geophys. Res.* **95**, 14095–14104. http://dx.doi.org/10.1029/JB095iB09p14095.

Shearer C. K., McKay G., Papike J. J. and Karner J. M. (2006) Valence state partitioning of vanadium between olivine-liquid: Estimates of the oxygen fugacity of Y980459 and application to other olivine-phyric martian basalts. *Am. Mineral.* **91**, 1657–1663.

Shearer C., Burger P., Papike J., Borg L., Irving A. and Herd C. (2008) Petrogenetic linkages among Martian basalts: Implications based on trace element chemistry of olivine. *Meteorit. Planet. Sci.* **43**, 1241–1258.

Silver P. G., Carlson R. W. and Olson P. (1988) Deep slabs, geochemical heterogeneity, and the large-scale structure of mantle convection – Investigation of an enduring paradox. *Ann. Rev. Earth Planet. Sci.* **16**, 477–541.

Smith P. M. and Asimow P. D. (2005) Adiabat_1ph: A new public front-end to the MELTS, pMELTS, and pHMELTS models. *Geochem. Geophys. Geosyst.* **6**, Q02004. http://dx.doi.org/10.1029/2004GC000816.

Socrates G. (2004) *Infrared and Raman Characteristic Group Frequencies: Tables and Charts*, third ed. Willey, New York.

Squyres S. W., Aharonson O., Clark B. C., Cohen B. A., Crumpler L., de Souza P. A., Farrand W. H., Gellert R., Grant J., Grotzinger J. P., Haldemann A. F. C., Johnson J. R., Klingelhöfer G., Lewis K. W., Li R., McCoy T., McEwen A. S., McSween H. Y., Ming D. W., Moore J. M., Morris R. V., Parker T. J., Rice J. W., Ruff S., Schmidt M., Schröder C., Soderblom L. A. and Yen A. (2007) Pyroclastic activity at Home Plate in Gusev Crater, Mars. *Science* **316**, 738–742.

Stanley B. D., Hirschmann M. M. and Withers A. C. (2011) CO_2 solubility in martian basalts and martian atmospheric evolution. *Geochim. Cosmochim. Acta.* **75**, 5987–6003.

Stevenson D. J. (2001) Mars' core and magnetism. *Nature* **412**, 214–219.

Stewart A. J., Schmidt M. W., van Westrenen W. and Liebske C. (2007) Mars: A new core-crystallization regime. *Science* **316**, 1323–1325.

Takahashi E. (1986) Melting of a dry peridotite KLB-1 up to 14 GPa: Implications on the oririn of peridotitic upper mantle. *J. Geophys. Res.* **91**, 9367–9382. http://dx.doi.org/10.1029/JB091iB09p09367.

Taylor L., Nazarov M., Shearer C., McSween H., Cahill J., Neal C., Ivanova M., Barsukova L., Lentz R., Clayton R. and Mayeda T. K. (2002) Martian meteorite Dhofar 019: A new shergottite. *Meteorit. Planet. Sci.* **37**, 1107–1128.

Tian F., Claire M. W., Haqq-Misra J. D., Smith M., Crisp D. C., Catling D., Zahnle K. and Kasting J. F. (2010) Photochemical and climate consequences of sulfur outgassing on early Mars. *Earth Planet. Sci. Lett.* **295**, 412–418.

Trønnes R. G. and Frost D. J. (2002) Peridotite melting and mineral–melt partitioning of major and minor elements at 22–24.5 GPa. *Earth Planet. Sci. Lett.* **197**, 117–131.

Tsuno K. and Dasgupta R. (2011) Melting phase relation of nominally anhydrous, carbonated pelitic-eclogite at 2.5–3.0 GPa and deep cycling of sedimentary carbon. *Contrib. Mineral Petrol.* **161**, 743–763.

Usui T., McSween, Jr., H. Y. and Floss C. (2008) Petrogenesis of olivine-phyric shergottite Yamato 980459, revisited. *Geochim. Cosmochim. Acta* **72**, 1711–1730.

Wadhwa M. (2001) Redox state of Mars' upper mantle and crust from Eu anomalies in shergottite pyroxenes. *Science* **291**, 1527–1530.

Walter M. J. (1998) Melting of garnet peridotite and the origin of komatiite and depleted lithosphere. *J. Petrol.* **39**, 29–60.

Wanke H. and Dreibus G. (1988) Chemical composition and accretion history of terrestrial planets. *Phil. Trans. R. Soc. A* **325**, 545–557.

Wendlandt R. F. (1982) Sulfide saturation of basalt and andesite melts at high pressures and temperatures. *Am. Mineral.* **67**, 877–885.

Williams J.-P. and Nimmo F. (2004) Thermal evolution of the Martian core: Implications for an early dynamo. *Geology* **32**, 97–100.

Wilson J. and Mustard J. (2013) Exposures of Olivine-rich rocks in the vicinity of Ares Vallis: Implications for Noachian and Hesperian volcanism. *J. Geophys. Res.* **118**, 916–929. http://dx.doi.org/10.1002/jgre.20067.

Xirouchakis D., Draper D. S., Schwandt C. S. and Lanzirotti A. (2002) Crystallization conditions of Los Angeles, a basaltic Martian meteorite. *Geochim. Cosmochim. Acta* **66**, 1867–1880.

Yoder C. F., Konopliv A. S., Yuan D. N., Standish E. M. and Folkner W. M. (2003) Fluid core size of Mars from detection of the solar tide. *Science* **300**, 299–303.

Yung Y. L., Nair H. and Gerstell M. F. (1997) CO_2 greenhouse in the early martian atmosphere: SO_2 inhibits condensation. *Icarus* **130**, 222–224.

Zhang J. and Herzberg C. (1994) Melting experiments on anhydrous peridotite KLB-1 from 5.0 to 22.5 GPa. *J. Geophys. Res.* **99**, 17729–17742. http://dx.doi.org/10.1029/94JB01406.

Zhang J., Li B., Utsumi W. and Liebermann R. C. (1996) In situ X-ray observations of the coesite-stishovite transition: Reversed phase boundary and kinetics. *Phys. Chem. Miner.* **23**, 1–10.

Zipfel J., Scherer P., Spettel B., Dreibus G. and Schultz L. (2000) Petrology and chemistry of the new shergottite Dar al Gani 476. *Meteorit. Planet. Sci.* **35**, 95–106.

Associate editor: Marc Norman